UNIVERSITI PUTRA MALAYSIA

PREPARATION OF REDUCED GRAPHENE OXIDE-BASED WORKING ELECTRODE AND COUNTER ELECTRODE FOR DYE-SENSITIZED SOLAR CELL APPLICATIONS

NOR FATHIN AINI BINTI JUMERI

FS 2015 19

PREPARATION OF REDUCED GRAPHENE OXIDE-BASED WORKING ELECTRODE AND COUNTER ELECTRODE FOR DYE-SENSITIZED SOLAR CELL APPLICATIONS

By

NOR FATHIN AINI BINTI JUMERI

Thesis Submitted to the School of Graduate Studies, Universiti Putra Malaysia, in Fulfilment of the Requirements for the Master of Science

September 2015

Abstract of thesis presented to the Senate of Universiti Putra Malaysia in fulfilment of the requirement for the Master of Science

PREPARATION OF REDUCED GRAPHENE OXIDE-BASED WORKING ELECTRODE AND COUNTER ELECTRODE FOR DYE-SENSITIZED SOLAR CELL APPLICATIONS

By

NOR FATHIN AINI BINTI JUMERI

September 2015

Chair: Janet Lim Hong Ngee, PhD

Faculty: Science

In this work, the enhancement of dye-sensitized solar cell (DSSC) using graphene-based materials for the making of working and counter electrodes was explored. Titanium dioxide (TiO_2) film was deposited on an indium tin oxide (ITO) glass by an in-house aerosol-assisted chemical vapour deposition method (AACVD). Graphene oxide (GO) was then introduced onto the TiO_2-ITO substrate by dip-coating and the layer of GO was successively thermally treated to reduced graphene oxide (rGO). The TiO_2-rGO film was used as a compact layer for the working electrode of the DSSC, which served as a blocking layer where it prevented the undesired back electron transfer and increased the photoconversion efficiency of DSSC. Compact layer was introduced in this work to overcome the issue of electrons recombination which caused the photocurrent loss and seriously decrease the photovoltaic performance of DSSC. A layer of zinc oxide-silver (ZnO-Ag) was introduced atop the compact layer as an active material by a dr. blade approach. The ZnO-Ag was synthesized using a microwave method and composed of a highly porous flower-shaped morphology, which was advantageous for adsorption of dye. An in-situ electrochemical polymerization method for the fabrication of polypyrrole nanoparticles incorporated reduced graphene oxide and *p*-toluenesulfonate (pTS) (Ppy-rGO-pTS) on a conducting ITO glass was used as a counter electrode for the platinum (Pt)-free DSSC since Pt material is one of the most expensive materials in DSSC. In addition, Ppy-rGO-pTS merits in excellent electron conductivity and high electrocatalytic activities. Cyclic voltrammetry (CV) was employed to determine the solar conversion efficiency. The efficiency of the ZnO-Ag-**TiO_2 photoanode in this work was far lower than the photoanode of ZnO-Ag-TiO_2-rGO owing to the presence of rGO, which** enhanced the electrochemical performance. The DSSC assembled with

the Ppy-rGO-1.0pTS counter electrode exhibited an enhanced power conversion efficiency of 1.99% under the solar illumination, as compared to using conventional Pt as a counter electrode (0.08%), which was attributed to the increased contact area between Ppy-rGO-pTS counter electrode and electrolyte, which also subsequently improved the conductivity of the Ppy-rGO-pTS counter electrode. The objectives of this work are to investigate the photocurrent performance of a working electrode, which composed of a titanium dioxide-reduced grapheme oxide (TiO_2-rGO) compact layer produced via aerosol assisted chemical deposition (AACVD) and dip-coating methods, and a zinc oxide-silver (ZnO-Ag) active layer produced via a microwave method, to assess the performance of a polypyrrole-reduced graphene oxide-p-toluenesulfonate (Ppy-rGO-pTS) counter electrode for a Pt-free DSSC and to study the efficiency of photovoltaic performance for ZnO-Ag-TiO_2-rGO as a working electrode and Ppy-rGO-pTS as a counter electrode. The as-fabricated DSSC exhibited novelty in terms of using Ppy-rGO-1.0pTS counter electrode as a promising alternative counter electrode for low-cost and high-efficiency DSSCs, and making use of rGO as an active material to enhance solar conversion.

Abstrak tesis yang dikemukakan kepada Senat Universiti Putra Malaysia
sebagai memenuhi keperluan untuk Master Sains

PENYEDIAAN ELEKTROD KERJA DAN ELEKTROD LAWAN BERASASKAN GRAFIN UNTUK PENGGUNAAN SEL SOLAR PEKA PENCELUP

Oleh

NOR FATHIN AINI BINTI JUMERI

September 2015

Pengerusi: Janet Lim Hong Ngee, PhD

Fakulti: Sains

Di dalam kerja ini, peningkatan sel solar peka pencelup (DSSC) dengan menggunakan bahan-bahan berasaskan grafin untuk membuat elektrod kerja dan elektrod lawan telah diselidik. Titanium dioksida (TiO_2) dimendapkan pada kaca indium timah oksida (ITO) menggunakan kaedah pemendapan wap kimia dengan bantuan aerosol (AACVD). Kemudian, Graphen oksida (GO) ditambahkan ke atas substrat TiO_2-ITO dengan menggunakan kaedah penyalutan celup dan lapisan GO telah melalui proses terma untuk menjadi grafin (rGO). Filem nipis TiO_2-rGO digunakan sebagai lapisan padat pada elektrod kerja untuk DSSC, bertindak sebagai lapisan penghalang di mana ia menghalang pemindahan elektron balik yang tidak diingini dan meningkatkan kecekapan foto penukaran DSSC. Lapisan padat diperkenalkan dalam kerja ini untuk mengatasi isu penggabungan semula elektron yang menyebabkan kerugian fotoarus dan mengurangkan prestasi fotovoltan DSSC. Lapisan zink oksida-perak (ZnO-Ag) diperkenalkan di atas lapisan padat sebagai bahan aktif menggunakan kaedah dr. blade. ZnO-Ag telah disintesis dengan menggunakan kaedah ketuhar gelombang mikro dan menghasilkan morfologi yang sangat berliang berbentuk bunga di mana ia berfaedah untuk penyerapan pencelup. Satu kaedah in-situ elektrokimia pempolimeran untuk menghasilkan nanopartikel polypyrrole digabungkan bersama grafin dan p-toluenesulfonate (pTS) (Ppy-rGO-pTS) pada kaca konduksi ITO telah digunakan sebagai elektrod lawan untuk DSSC bebas platinum (Pt) kerana bahan Pt merupakan salah satu bahan yang paling mahal di dalam DSSC. Disamping itu, sifat Ppy-rGO-pTS yang cemerlang dalam mengkonduksi elektron dan aktiviti electro pemangkin. Voltrammetri berkitar (CV) telah digunakan untuk menentukan kecekapan penukaran solar. Kecekapan fotoanod ZnO-Ag-TiO_2 yang dipamerkan di dalam kerja ini adalah jauh lebih rendah daripada fotoanod ZnO-Ag-TiO_2-rGO kerana kehadiran rGO yang telah meningkatkan prestasi elektrokimia. DSSC yang dipasang dengan Ppy-rGO-1.0pTS elektrod lawan

mempamerkan peningkatan kecekapan penukaran kuasa sebanyak 1.99% di bawah pencahayaan solar, berbanding Pt konvensional sebagai elektrod penghalang (0.08%), hal ini dikaitkan dengan peningkatan sentuhan kawasan di antara Ppy-rGO-pTS elektrod lawan dan elektrolit, di mana ia juga meningkatkan kekonduksian Ppy-rGO-pTS elektrod lawan. Objektif kerja ini adalah untuk menyelidik prestasi fotoarus elektrod kerja, yang terdiri daripada lapisan padat TiO_2-rGO dan lapisan aktif ZnO-Ag, untuk menilai prestasi Ppy-rGO-pTS elektrod lawan di dalam DSSC bebas Pt dan untuk mengkaji kecekapan prestasi fotovoltan ZnO-Ag-TiO_2-rGO sebagai elektrod kerja dan Ppy-rGO-pTS sebagai elektrod lawan. Rekaan-DSSC mempamerkan sesuatu yang baru dari segi penggunaan Ppy-rGO-1.0pTS elektrod lawan sebagai salah satu alternatif elektrod lawan yang menjanjikan kos rendah dan kecekapan DSSCs yang tinggi, dan penggunaan grafin sebagai bahan aktif untuk meningkatkan penukaran solar.

ACKNOWLEDGEMENTS

I would like to express my deep and sincere gratitude to many people who made this MSc. thesis possible. Firstly, I would like to express my gratefulness to my supervisor, Dr. Janet Lim Hong Ngee for leading me into the exciting material chemistry field, for encouraging me to be creative and think deeper, and advising me to try different ideas. Her softness along with the excellent guidance in research not only made me learn many techniques and understanding in research but also, I enjoyed the work in the laboratory.

I am highly indebted to my committee members Prof. Dr. Zulkarnain Zainal, Dr. Huang Nay Ming, Dr. Pandikumar and Ms Lim Su Pei. Their ideas, encouragement and help to do the best research cannot be eclipsed. It is not an exaggeration to say that I could not reach this far without their generous help.

I owe my deepest gratitude to my family for the endless support and unconditional love. Without their encouragement and understanding it would have been impossible for me to finish this work. Finally, special thanks to Afiq Ali, for his understanding during the past few years.

My gratitude is also extended to all my colleagues, especially Mr. Chee Wei Kit, Ms. Asilah Jamil, and Ms. Siti Normaimunah Ariffin for sharing the laughter and tears during this period of time. Not forgetting to show my appreciation to Fundamental Research Grant Scheme (FRGS) and Research Management Centre (RMC) of UPM for providing financial support which was very crucial for my study.

I certify that a Thesis Examination Committee has met on (date of viva voce) to conduct the final examination of (student's name) on his (her) thesis entitled ("Title of Thesis") in accordance with the Universities and University Colleges Act 1971 and the Constitution of the Universiti Putra Malaysia [P.U.(A) 106] 15 March 1998. The Committee recommends that the student be awarded the (insert the name of relevant degree).

Members of the Thesis Examination Committee were as follows:

Name of Chairperson, PhD
Title (e.g., Professor/Associate Professor/Ir; omit if irrelevant)
Name of Faculty
Universiti Putra Malaysia
(Chairman)

Name of Examiner 1, PhD
Title (e.g., Professor/Associate Professor/Ir; omit if irrelevant)
Name of Faculty
Universiti Putra Malaysia
(Internal Examiner)

Name of Examiner 2, PhD
Title (e.g., Professor/Associate Professor/Ir; omit if irrelevant)
Name of Faculty
Universiti Putra Malaysia
(Internal Examiner)

Name of External Examiner, PhD
Title (e.g., Professor/Associate Professor/Ir; omit if irrelevant)
Name of Department and/or Faculty
Name of Organisation (University/Institute)
Country
(External Examiner)

_____
(Insert name of current Deputy Dean)
(E.g. XXXXX XXXX, PhD)
Professor and Deputy Dean
School of Graduate Studies
Universiti Putra Malaysia

Date:

This thesis was submitted to the Senate of Universiti Putra Malaysia and has been accepted as fulfilment of the requirement for the Master of Science. The members of the Supervisory Committee were as follows:

Janet Lim Hong Ngee, PhD
Senior Lecturer
Faculty of Sciene
Universiti Putra Malaysia
(Chairman)

Zulkarnain Zainal, PhD
Professor
Faculty of Science
Universiti Putra Malaysia
(Member)

_____
BUJANG BIN KIM HUAT, PhD
Professor and Dean
School of Graduate Studies
Universiti Putra Malaysia

Date:

Declaration by graduate student

I hereby confirm that:

- this thesis is my original work;
- quotations, illustrations and citations have been duly referenced;
- this thesis has not been submitted previously or concurrently for any other degree at any other institutions;
- intellectual property from the thesis and copyright of thesis are fully-owned by Universiti Putra Malaysia, as according to the Universiti Putra Malaysia (Research) Rules 2012;
- written permission must be obtained from supervisor and the office of Deputy Vice-Chancellor (Research and Innovation) before thesis is published (in the form of written, printed or in electronic form) including books, journals, modules, proceedings, popular writings, seminar papers, manuscripts, posters, reports, lecture notes, learning modules or any other materials as stated in the Universiti Putra Malaysia (Research) Rules 2012;
- there is no plagiarism or data falsification/fabrication in the thesis, and scholarly integrity is upheld as according to the Universiti Putra Malaysia (Graduate Studies) Rules 2003 (Revision 2012-2013) and the Universiti Putra Malaysia (Research) Rules 2012. The thesis has undergone plagiarism detection software.

Signature: _____ Date: _____

Name and Matric No.: _____

Declaration by Members of Supervisory Committee

This is to confirm that:

- the research conducted and the writing of this thesis was under our supervision;
- supervision responsibilities as stated in the Universiti Putra Malaysia (Graduate Studies) Rules 2003 (Revision 2012-2013) are adhered to.

Signature: _____
Name of Chairman of Supervisory Committee: _____

Signature: _____
Name of Member of Supervisory Committee: _____

Signature: _____
Name of Member of Supervisory Committee: _____

Signature: _____
Name of Member of Supervisory Committee: _____

TABLE OF CONTENTS

LIST OF TABLES

LIST OF FIGURES

LIST OFABBREVIATIONS/ NOTATIONS

AACVD	Aerosol-assisted Chemical Vapour Deposition
AFM	Atomic Force Microscopy
CA	Chronoammperometry
CE	Counter electrode
CNTs	Carbon nanotubes
CV	Cyclic voltammetry
CVD	Chemical Vapour Deposition
DSSC	Dye-sensitized Solar Cell
EIS	Electrochemical impedance spectroscopy
FESEM	Field emission scanning electron microscopy
FF	Field factor
FTO	Fluorine-doped tin oxide
hv	Harvest light energy
Is	Solar light intensity
ITO	Indium tin oxide
Jmax	Maximum current
Joc	Open circuit current
Jsc	Short circuit current
J-V	Photocurrent-Voltage
LSV	Linear Sweep Voltammetry
LUMO	Lowest unoccupied molecular orbital
MWCNT	Multi-walled carbon nanotube

PIFCO	Piezoelectric modulator of an ultrasonic humidifier
P25	Titanium dioxide type P25
RE	Reference electrode
Rct	Charge-transfer resistance at counter electrode-dye electrolyte interface
Rpt	Charge-transfer resistance at working electrode electrolyte interface
SEM	Scanning electron microscopy
SSPs	Single-source precursors
TEM	Transmission electron microscopy
VLS	Vapor-liquid-solid
Vmax	Maximum voltage
Voc	Open circuit voltage
Vsc	Short Circuit Voltage
WE	Working electrode
XRD	X-ray diffraction

CHAPTER 1

INTRODUCTION

1.1 Background of Study

A dye-sensitized solar cell (DSSC) has become one of the most promising new generation solar cells since its invention in 1991 by O'Regan and Gretzel (O'Regan and Graetzel, 1991). Solar energy is one of the most important, green, and reproducible energy sources as an alternative to traditional fossil fuels from the perspective of a sustainable economy. DSSCs have attracted tremendous attention from many researchers because of their low cost, light weight, moderate efficiency, flexibility, and easy fabrication (Han *et al.*, 2014; Yang *et al.*, 2014; Babu *et al.*, 2015). Typically, standard DSSCs consist of a dye-sensitized mesoporous semiconductor photoanode, an iodide/tri-iodide (I_3^-/I^-) redox electrolyte, and a catalytic counter electrode. The counter electrode is an important component of a DSSC, and has roles that include collecting electrons from the external circuit and reducing I_3^- to I^- in the electrolyte. Usually fluorine-doped tin oxide (FTO) glass is loaded with platinum to facilitate electron transfer from the external circuit to the I_3^-/I^- redox electrolyte because of the high catalytic activity and conductivity of platinum (Sun *et al.*, 2012).

For the past few decades, a large number of studies have focused on the potential application of metal oxide semiconductor materials for solar energy conversion. Among the range of semiconductors available, TiO_2-based materials are the most popular, and considerable progress has been achieved (Kwak *et al.*, 2014). The energy gap of the TiO_2 conduction band and the excited-state energy gap of dye molecules are quite close. Under irradiation, the electrons produced after dye is excited can very easily step rapidly from the energy gap of the lowest unoccupied molecular orbital (LUMO) to the TiO_2 conduction band, which has a lower energy gap. Therefore, TiO_2 nanoparticles have always typically been used as the photoelectrode material of a DSSC. The TiO_2 thin film commonly used in a DSSC is made of TiO_2 nanoparticles for commercial use. Moreover, because TiO_2 powder has a granular structure, when electrons are transported among particles, this leads to electron scattering, which causes an energy loss and affects the photoelectric conversion efficiency of the DSSC (Chang *et al.*, 2013). A TiO_2 compact layer has drawn much attention in recent years (Yang *et al.*, 2014). A TiO_2 compact layer has been widely used as a photoelectrode in the DSSC area, and it has been reported that TiO_2 can greatly decrease the back reaction sites on ITO and improve the short-circuit current (*Jsc*) of DSSCs (Abdullah and Rusop, 2013; Wang *et al.*, 2014; Yang *et al.*, 2014). In addition, a TiO_2 compact film has also been used to investigate the effects of electron diffusion (Gao *et al.*, 2014). TiO_2 is a strong candidate due to its high stability in aqueous solutions and high photovoltaic and photocatalytic activity. Their excellent ability to harvest light energy (*hv*), and extremely high surface area brought about tubular structures as ideal structures to achieve high photocatalytic properties.

TiO_2 is an excellent photocatalyst for the treatment of harmful organic pollutants (Zhang *et al.*, 1998).

In typical aerosol-assisted chemical vapor deposition (AACVD) process, the aerosol of the precursor solution, generated using piezoelectric transducer, is transferred to the heated zone using carrier gas, where it decomposes to give the final product on the surface of substrate (thin film) (Hussain *et al.*, 2012). Aerosol assisted chemical vapor deposition (AACVD) at atmospheric pressure presents some key advantages, including a wider choice and availability of precursors for high quality CVD products, mass production, high deposition rate, improvement of precursor selection and stoichiometric control. Generally with AACVD process and after decomposition, organic residua and hydroxyl groups will still remain on the top of the films surface and their presence is inevitable (Salhi *et al.*, 2011; Elleuch *et al.*, 2013). AACVD is an attractive method as it uses single-source precursor. Besides, advantage of AACVD is that non-volatile precursor may be used for depositing (Hou and Choy, 2006). AACVD diminishes the stringent CVD requirement for the precursor to be highly volatile: it is only required to be soluble in a solvent from which an aerosol can be generated (Ehsan *et al.*, 2011). Moreover, it provides a greater capability and flexibility than conventional CVD because of its simple and good control of the transport of the precursor to the deposition zone (Cholula-Díaz *et al.*, 2014). AACVD is able to obtain high-quality homogenous thin films with a strong adherence to the substrate (Fa *et al.*, 2014). However, the porosity on the surface of the TiO_2 is low, and the dye absorption decreases.

In addition, graphene, as a UV stabilizer, has also been introduced with TiO_2 to absorb as much sunlight as possible and easily donate the captured electrons from the dye molecules to the external surface of the semiconductor film. Graphene has attracted considerable attention lately because of its unique characteristics (Kwak *et al.*, 2014). The special two-dimensional honeycomb crystal structure of graphene enables numerous excellent characteristics for a DSSC, including a larger surface area, chemical stability, high transmittance, and electrical conductivity (Qiu *et al.*). Graphene is a uniform and thin transparent conducting material with unique electrical, thermal and mechanical properties (Wang *et al.*, 2011). It has shown many intriguing properties including a strong ambipolar electric-field effect such that electrons and holes in concentrations up to 10^{13} cm^{-2} and with room temperature mobilities ≈10,000 cm^2/Vs can be induced by applying gate voltage (Novoselov *et al.*, 2004), specific surface area of up to >2600 m^2/g (Jang and Zhamu, 2008), unique transport performance, high mechanical strength, extremely high thermal conductivity (Wang *et al.*, 2009), electrochemical and unconventional nanomagnetic properties (Rao *et al.*, 2009).

The TiO_2-rGO composite materials have been used previously for photocatalytic and photoconduction applications. This type of nano-composites have also been employed for dye sensitized solar cells and electrochemical water splitting (Sharma *et al.*, 2014). In typical TiO_2-based DSSCs,

photogenerated electrons transport through mesoporous TiO_2 films to electrode for collection. The high charge-collection efficiency requires fast electron transport to avoid the recombination with the reduced redox species. To improve the charge-collection efficiency, one promising solution is to introduce highly electrically conductive carbon materials, such as graphene into TiO_2 (Zhu *et al.*, 2014).

Zinc Oxide (ZnO) is already used in all-solid state solar cells as a n-type window material (Lee *et al.*, 2000; Nishi *et al.*, 2013; Minami *et al.*, 2014). ZnO with various morphologies has been used in DSSCs, although the power conversion efficiencies obtained in ZnO-based DSSCs is significantly lower in most cases compared to TiO_2-based cells (Jana *et al.*, 2014). Furthermore, ZnO has also been considered to be a promising candidate, because it exhibits a higher electron mobility than TiO_2 (Li *et al.*, 2010). In order to be used as an electrode material in a DSSC, it must be introduced as a porous film several microns thick with a very high surface area to allow the absorption of a large amount of dye molecules (Dupuy *et al.*, 2010). A microwave-assisted method has been reported to result in ZnO with high porosity (Ma *et al.*, 2013; Ashok and Venkateswara Rao, 2014; Liang *et al.*, 2014). The advantages of microwave heating include an instantaneous and fast heat-up time and easy control, because the microwave energy is delivered directly to the material through interactions at the molecular level with the electromagnetic field. Microwaves penetrate the material and provide energy, resulting in volumetric heating (Ul Haq *et al.*, 2015). Moreover, the microwave method also provides reduced energy consumption, rapid heating rates, reduced sintering times, enhanced element diffusion processes, and improved physical and mechanical properties for the sintered materials (Xu *et al.*, 2015) Further, ZnO has higher electron mobility (115–155 $cm^2 V^{-1} S^{-1}$) and allows simpler fabrication of various nanostructures, which are benefits for the electron transport and allows the performance to be optimized by altering the nanostructures. Therefore, ZnO is considered to be one of the most promising materials for DSSCs (Lou *et al.*, 2013).

Among the noble metal materials widely used in hybrid nanostructures is Ag. The combination of Ag nanoparticles with ZnO nanorods can offer unique optical, electronic, and thermal characteristics (Khan *et al.*, 2014). Ag acts as not only electron sinks but also as charge carrier recombination centers in Ag/ZnO composites (Ren *et al.*, 2010). Furthermore, it was also observed that Ag nanoparticles can promote the formation of active hydroxyl radicals on the surface of ZnO (Lu *et al.*, 2014). Thus, modification of ZnO using Ag has been extensively investigated and become one of the most popular approaches for enhancing the photocatalytic efficiency in UV and visible light conditions (Liu *et al.*, 2015). Moreover, the modification of ZnO by noble metals such as silver has attracted significant attention because noble metal can be used as a scavenger for photogenerated electrons, promoting interfacial electron–hole separation in the photocatalytic process, thereby increasing the number of photocharges and improving the photocatalytic activity (Bechambi *et al.*).

Currently, the most widely used counter electrodes in DSSCs are fluorine-doped tin oxide (FTO) or indium-doped tin oxide (ITO) glass substrates coated with platinum (Pt). However, the cost and problem of Pt dissolution in a corrosive electrolyte have restricted their large-scale application to DSSCs (Yue *et al.*, 2014). Therefore, the replacement for Pt as a low-cost counter electrode is polypyrrole nanoparticles incorporating graphene oxide (PPy-GO) (Yue *et al.*, 2014). Activated carbon and graphite have been used to fabricate supercapacitors because of their good stability, but these microstructures limit the capacitance value. PPy can also be employed as a charge storage material that possessed high capacitance. This concept can be used to construct a DSSC with inherent charge storage capacity (Saranya *et al.*, 2015). PPy-GO has been tested in supercapacitor electrodes and high capacitances, and has been shown to also improve the PPy stability (Sun and Mo, 2013). The results reveal that the capacitance of the electrodes with a rough surface is several hundred times higher than that of a smooth Pt surface (Norlin *et al.*, 2002). So in this case, it is found that after the deposition of PPy on GO sheets, increased the rough surfaces which could be beneficial to obtain efficient conductivity, where it is crucial to gain high electrocatalytic activity for counter electrode (Yue *et al.*, 2014) subsequently improved the mechanical property of PPy, and enhanced the electrical conductivity (Fan *et al.*, 2014). The specific capacitance value could be enhanced from 108 to 289 F g^{-1} at a constant current density of 1 A g^{-1} through the electrochemical incorporation of GO in a PPy film (Qi *et al.*, 2014) that makes it a promising candidate as counter electrode materials used in DSSC, because of their unique properties, such as inexpensive, high conductivity, remarkable stabilities, good specific capacitances, and catalytic activity for I_2 reduction (Wu *et al.*, 2008). Generally, Ppy has low crystallinity and anisotropy. In contrast to the PPy deposited from solutions containing small inorganic anions, films deposited in the presence of such aromatic anions as *p*-toluenesulfonate (pTS) exhibit an anisotropic molecular organization. Therefore, high conductivity (as obtained for electrodeposited PPy films doped with some organic anions) results in the polymer having a well-packed structure (Raudsepp *et al.*, 2010).

1.2 Problem Statement

Over recent years, solar cells have become important sustainable green energy alternatives to fossil fuels. Among which, dye-sensitized solar cell (DSSC) has gained considerable attention due to its potential of low fabrication cost and high power conversion efficiency. A typical DSSC is composed of a dye-adsorbed metal oxide layer deposited on ITO as the working photoelectrode, a platinized counter electrode and a liquid electrolyte containing iodide/triiodide I^-/I_3^- redox couple. At these interfaces, photogenerated electrons may recombine with the oxidized species (such as I_3^- in the redox electrolyte or dye cations), which caused the photocurrent loss and seriously decrease the photovoltaic performance of DSSC (Fang *et al.*, 2014). To overcome this issue and to improve the performance of the device, compact layer has been introduced (Sun *et al.*, 2014). It is vital to introduce an effective compact layer onto the ITO glass to block the electron recombination (Fang *et al.*, 2014).

Apart from that, platinum (Pt) is still the most widely-used counter electrode for DSSCs. However, the Pt material is one of the most expensive materials in DSSCs and can be decomposed to PtI_4 by I^-/I_3^- redox couple, thus resulting in the critical issues on the cell performance, long-term stability, and commercialization of DSSCs (Ghani *et al.*, 2015). In order to resolve the issues, several catalytic materials have been studied, such as carbon materials, conducting polymers, and composite materials (Yue *et al.*, 2014). Conductive polymers such as Ppy is very promising alternatives for counter electrode materials in DSSCs because of their unique properties such as affordability, good stability, and higher catalytic activity for I_3^- reduction (Peng *et al.*, 2011; Saranya *et al.*, 2015). Nonetheless, in order to further improve the conductivity performances of DSSC, Ppy-rGO seem to be good candidates of the electrode materials. rGO probably further enhances the capacitive performances of PPy because of high electrical conductivity and high specific surface area (Peng *et al.*, 2014). In addition, the electrochemical performance and stability of the PPy-rGO composites improved through doping of pTS anion in the PPy matrix (Sultana *et al.*, 2012). Thus, Ppy-rGO-pTS counter electrode has been introduced for Pt-free DSSC application.

1.3 Objectives of the study

Dye sensitized solar cells (DSSCs) have attracted considerable attention in solar cell research community. It is low-cost, easy manufacturing process and possible flexible device fabrication (Bhande *et al.*, 2014). This work highlights about the introduction of reduced graphene oxide (rGO) on the compact layer of working electrode and counter electrode for the Pt-free DSSC. The objectives of this work were as follows:

1. To investigate the photocurrent performance of a working electrode, which composed of a titanium dioxide-reduced graphene oxide (TiO_2-rGO) compact layer via aerosol assisted chemical deposition (AACVD) and dip coating methods as well as zinc oxide-silver (ZnO-Ag) active layer via microwave method.
2. To access the performance of polypyrrole-reduced graphene oxide-p-toluenesulfonate (Ppy-rGO-pTS) counter electrode for the Pt-free for DSSC application.
3. To study the efficiency of photovoltaic performance for ZnO-Ag-TiO_2-rGO as working electrode and Ppy-rGO-pTS as counter electrode.

1.4 Scope of Research

This thesis describes the improvement of photovoltaic efficiency using reduced graphene oxide-based working and counter electrodes. A TiO_2-rGO compact layer working electrode was described in detail, which include its technique of fabrication and subsequent analysis. Furthermore, the fabrication of ZnO-Ag active layer on the TiO_2-rGO compact layer working electrode was described, using Ppy-rGO-pTS as a counter electrode material. These combination of materials enabled the realisation of Pt-free DSSCs.

CHAPTER 2

LITERATURE REVIEW

2.1 Graphene vs. Reduced Graphene Oxide (rGO)

Graphene is a two-dimensional (2D) sp^2 bonded carbon sheet, arranged in a hexagonal honeycomb lattice (Chen *et al.*, 2015; Gadipelli and Guo, 2015). From a fundamental point of view, graphene is a single layer of graphite, which is an infinite three-dimensional (3D) material made up of stacked layers of graphene. The layers in graphite interact weakly through van der Waals (vdW) forces. In terms of properties graphene is unique; it is a soft membrane and at the same time possesses a high Young's modulus, and good thermal and electrical conductivities (Abergel *et al.*, 2010; Gadipelli and Guo, 2015). Graphene has attracted considerable interest over the last few years on account of its extraordinary electrical, thermal, and mechanical properties arising from its unique structure (Liu *et al.*, 2015). It has high thermal conductivity (5300 W/mK) and electrical conductivity (2000 S/cm) and in addition, it has the fastest electron mobility (de Moraes *et al.*, 2015). It is 30 times harder than diamonds and 200 times harder than steel. Moreover, it also has interesting optical properties and can absorb about 2.3% of white light which makes it an excellent choice for the production of more efficient solar cells (Aghigh *et al.*, 2015). With all of the mentioned advantages, there is a problem with graphene and it is that a band gap is not present and thus it can never be switched off and thus an engineered band gap needs to be implemented so that it can be used in different applications. Apart from this, due to the defects introduced during the exfoliation time, high quality graphene is hardly obtainable (Aghigh *et al.*, 2015; Liu *et al.*, 2015).

Reduced graphene oxide (rGO) is generally obtained via reduction of GO (Huang *et al.*, 2015). Reduced graphene oxide (rGO) can be produced in large scale and low cost. The residual oxygen-containing functional groups on rGO provide it with some aqueous dispersity and also offer anchors for further chemical modification. Considering the surface functional groups, together with its large specific surface area, rGO is considered as an ideal two dimensional carbon support for developing highly efficient catalysts (Yang *et al.*, 2015). Incorporating semiconductor nanocrystals with rGO not only can reduce the restocking of ultrathin graphene sheets, but also can prevent the aggregation and photocorrosion of nanocrystals (Zhang *et al.*, 2015). rGO sheets can obtain an increased conductivity compared with GO sheets owing to the restoration of the conjugated network in the rGO sheets. Considering the surface functional groups, together with its large specific surface area, rGO is considered as an ideal two dimensional carbon support for developing highly efficient catalysts. In addition, the use of metal nanoparticles as decorations on the rGO support can increase the distance between the rGO sheets and inhibit adhesion of the resulting rGO sheets in dry state, leading to the great improvement of dispersibility of the obtained nanocomposites. Furthermore, nanocomposites produced by the association of rGO with noble metal nanoparticles are expected to improve the catalytic performance and sensing property for the modified electrodes (Li *et al.*, 2015).

2.2 Synthesis Method of graphene and rGO

The discovery of graphene and its derivatives has opened a new era in the field of physics and materials science. The outstanding optical, electronic, thermal and mechanical properties shown by this material have created expectations regarding various possible applications. Different methods have been employed for the production of graphene and its derivatives. Mechanical exfoliation of graphite crystals was the first method reported by (Novoselov *et al.*, 2004). Although the quality of graphene produced in this way is excellent; the quantity of graphene that can be obtained is minimal and can only be used for fundamental studies. This is why other methods such as chemical vapor deposition (CVD) or chemical methods have been continually developed in response to the increasing demand for graphene materials.

Chemical vapor deposition (CVD) is the approach to produce good-quality and large-scale graphene layers. Control of the nucleation and growth of graphene during the CVD process is important to achieve large-scale and high-quality graphene layers. Tuning the C:H ratio, changing the hydrocarbon and H_2 gas pressures, and smoothing the substrate surface before growth have been used to grow graphene with desirable quality. However, the crucial growth parameters for graphene still remain unknown or uncontrolled (Li *et al.*, 2014).

Meanwhile, based from the study done by (Park and Ruoff, 2009), chemical methods have been proposed as a cheaper alternative and with higher production capacity than chemical vapor deposition. One of these methods is the production of graphene oxide (GO) by the oxidation of graphite. The oxidation of graphite allows the exfoliation of graphene oxide layers. This method involves oxidation of graphite to GO using highly oxidizing agent ($KMnO_4$) and subsequently reducing GO to graphene using hydrazine solvent. The main advantage of this synthesis method over other methods is that formation of a large quantity of graphene through a reduction step to convert the insulating GO into conducting reduced graphene oxide (rGO). Furthermore, rGO could be dispersed in both polar and non-polar solvents which contains =O stretching, C–O–C stretching, C–O stretching, and broad band for hydroxyl functional group (Pan *et al.*, 2014; Low *et al.*, 2015). This method presents an extremely simple, environment-friendly, and cost-effective method to both selectively reduce GO and to prepare rGO, which has a high specific surface (Pan *et al.*, 2014).

Furthermore, the oxygen-containing functional groups of GO are very useful in attaching inorganic nanoparticles within graphene sheets. However, these functional groups act as scattering centers and alter the sp^2 in-plane bonding, thereby reducing the optical and electrical properties of graphene. Hence, regaining sp^2 aromaticity by reducing these functional groups becomes necessary to enable reduced GO (rGO) to be effectively used as an efficient charge carrier shuttle and a photocatalytic support material (Kaveri *et al.*, 2013).

2.3 History of Dye-Sensitized Solar Cell (DSSC)

Solar energy is the source of nearly all energy on earth. Among all the renewable power sources, solar energy is the most easily exploitable, inexhaustible, quiet, and adjustable to enormous applications (Ludin *et al.*, 2014).

Solar cell technologies have evolved into three generations. First generation solar cells are based on a single crystalline semiconductor wafer. Second generation solar cells utilize inorganic thin film structure in the cell assembly (Abdin *et al.*, 2013; Parisi *et al.*, 2014). They are cheaper to produce, but their applications are limited due to either cost ineffective or hazardous materials used in these technologies. Thus, a new solar cell technology is required to achieve greater efficiencies with lower production cost. The onset of this breakthrough is the third generation solar cells. Currently, the focus is on the third generation solar cells that can deliver economic, highly efficient cells that can emerge as a new technology in the near future, such as multilayer or tandem cell (Conibeer *et al.*, 2006).

It was discovered that illuminated organic dyes can generate electricity at oxide electrodes in electrochemical cells, but somehow it showed very poor conversion (Gerischer *et al.*, 1968). Since then much effort has been put in to improve the power conversion efficiency. Major breakthrough came in when Prof. O'Regan and Grätzel of Swiss Federal Institute of Technology reported a DSSC device with an efficiency of 7.1% (O'Regan and Gratzel, 1991). The device was composed of a porous layer of titanium dioxide nanoparticles covered with a molecular dye (usually a Ru(II)–polypyridyl complex), which absorbs sunlight, like the chlorophyll in green leaves. The titanium dioxide is immersed under an electrolyte solution, above which is a platinum-based catalyst. As in a conventional alkaline battery, an anode (titanium dioxide) and a cathode (platinum) are placed on either side of a liquid conductor (electrolyte) (Benedetti *et al.*, 2012; Zhong *et al.*, 2012). Thereafter, much effort has been put in to improve the power conversion efficiency. Moreover, it did not take much time for the scientific community to prove the dye-sensitized solar cells are alternatives to the conventional first- and second-generation silicon solar cells. In fact, the DSSC technology works well. It is a promising device for using solar energy because of its low production cost compared to those of conventional semiconductor solar cells, and also its high light to electricity conversion efficiency (Meng *et al.*, 2015) even in diffused light conditions, unlike the first- and second-generation photovoltaic devices.

2.4 Types of Compact Layers for DSSC

In the past decades, a few metal oxide materials have been explored as a compact layer such as TiO_2 (Kovash Jr *et al.*, 2012; Abdullah and Rusop, 2013; Abdullah and Rusop, 2014), ZnO (Huang *et al.*, 2012; Yang *et al.*, 2014), SnO_2 (Duong *et al.*, 2013; Shaikh *et al.*, 2015) and CuO (Raksa *et al.*, 2009; Sahay *et al.*, 2012).

Since a decade ago, TiO_2 compact layer has been introduced between the indium thin oxide (ITO) and mesoporous metal oxide layer to retard the charge recombination of photo-injected electrons with I_3^- ions at the ITO/electrolyte interface (Guai *et al.*, 2013; Abdullah and Rusop, 2014; Sun *et al.*, 2014) and improve the short-circuit current (*Jsc*) of DSSCs greatly (Wang *et al.*, 2010). TiO_2 thin films can be produced using a variety of techniques like solvothermal synthesis or sol–gel methods, hydrothermal methods and chemical vapor deposition (CVD) to produce a porousity TiO_2 which is ideal for dye absorption (Kuo *et al.*, 2014) and improve the DSSC performance (Menzel *et al.*, 2012).

Similarly, ZnO compact layers improve open-circuit photovoltage and fill factor, and keep fairly good short-circuit photocurrent density (Huang *et al.*, 2012). It is reported that the ZnO compact films can form an energy barrier between ITO substrate and TiO_2 film due to more negative conduction band edge of ZnO than that of TiO_2 which would suppress recombination reaction and also improve *Voc* (Yang *et al.*, 2014).

SnO_2 is a n-type semiconductor oxide with a 3.8 eV band gap that is also a promising compact layer candidate that plays a role as blocking layer. SnO_2 is transparent, chemically stable, and has high electron mobility (100–200 cm^2/Vs) (Yong *et al.*, 2014). The high electron mobility in SnO_2 promotes faster transportation of photo-injected electrons in the conducting current collector (Shaikh *et al.*, 2015).

Moreover, CuO is also has been used as blocking layer. Copper oxides (CuO) is a few p-type metal–oxide semiconductors with a narrow band gap of 1.2 eV and a monoclinic crystal structure. It has received much attention due to a wide range of potential applications such as photoconductive, photothermal, catalysis and gas sensor (Zhang *et al.*, 2014). The enhancement of the power conversion efficiency of DSSC can be explained in terms of the retardation of the interfacial recombination dynamics of CuO blocking layer (Raksa *et al.*, 2009). By inserting the CuO blocking layer, the reaction possibilities of I^-/I_3^- with the photo-injected electrons to ITO substrate are significantly hindered, as demonstrated by the reduced dark current (Habibi *et al.*, 2013). The photocurrent with the incorporation of CuO nanofibers as a blocking layer increased since CuO blocking layer helped the retardation of the interfacial recombination, it is also the reason for the reduction in the reverse current thus improving the current density. This phenomenon was possible as the conduction band edge of CuO creating a potential gradient, which allowed the forward movement of electron leading to the low reverse current (Sahay *et al.*, 2012).

2.5 Types of Method to Produce Working Electrodes for DSSC Application

2.5.1 TiO_2 Working Electrode

Since its invention in 1991, the dye-sensitized solar cell (DSSC) has attracted significant attention as a promising photovoltaic device due to its low cost and convenience in fabrication (Liang *et al.*, 2015).

The working electrode is generally a wide band-gap semiconductor such as TiO_2 and ZnO others. It may be n-type or p-type. Mostly n-type is used due to its higher efficiency. Working electrode generally absorbs light in the ultraviolet region. The dye is generally an organometallic compound which is spread over a working electrode as a monolayer. In DSSC, the electron–hole pair is not separated by built in potential, but by assigning charge generation and separation function to different materials. Dye absorbs light in the visible region and generates an excited electron which is transferred to TiO_2 in picoseconds. This electron is transferred to the external circuit. The redox couple usually iodide/triiodide (I^-/I_3^-) dissolved in acetonitrile donates its electron to the dye and regenerates it. The oxidized species of electrolyte are reduced at the counter electrode (Saranya *et al.*, 2015).

Among the working electrode materials, titanium dioxide (TiO_2) has been considered one of the most promising photocatalytic materials due to its unique properties including relatively low cost, non-toxicity, chemical stability, and high photo stability (Li *et al.*, 2013). However, the efficiency of DSSC is very low in the visible light region due to the wide band gap of TiO_2 (3.2 eV for anatase phase) and the electron–hole pairs in the reaction can only be excited by the ultraviolet (UV) light (about 4% of the incoming solar energy). To overcome this limitation, a dye-sensitizer can help move the charge to TiO_2 by absorbing visible light at 500–600 nm, and injecting electrons. The production cost of DSSC is 30% that of traditional silicon solar cells, and theoretically, the conversion efficiency can be increased to 10-11% with less environmental damage (Wang *et al.*, 2006; Chae *et al.*, 2010).

The sol–gel process which is one of the simplest methods offers many advantages such as controllability, reliability, reproducibility of the material and therefore can be selected for the preparation of high quality nano-structured thin films (Lewkowicz *et al.*, 2014). The sol-gel process is a method for producing solid materials from small molecules. This method requires a simple set up and it is effective. In this process, the titania precursor undergoes hydrolysis and condensation reactions leading to the formation of an interconnected titanium dioxide network. The conditions for preparing TiO_2 thin films using the sol–gel process can strongly affect the physical properties of the film. (Brinker *et al.*, 1991). Meanwhile, the FE-SEM micrograph of TiO_2 films annealed at 400 °C is shown in **Fig. 1**. The top-view micrograph shows well-defined randomly oriented grains. The grains are closely packed without any visible pores between them. From the cross-sectional view, the thickness of the films was found to be ~280 nm with good uniformity (Meher and Balakrishnan, 2014). Apart from that, with the increase in annealing temperature, the morphology of the TiO_2 thin films changed gradually. The increase in temperature decreased the concentration of the binders, hence the aggregation between nanocrystallites was reduced. Thus, as the temperature increased, the growth and size distribution of the nanocrystallites were enhanced and the boundaries between particles were pronounced (Ranjitha *et al.*, 2013).

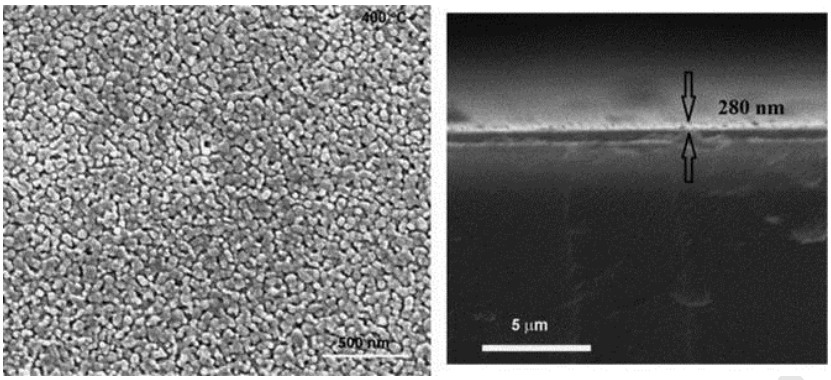

Fig. 1. FE-SEM figures (top-view and cross-sectional view) of TiO_2 films annealed at 400 °C (Meher and Balakrishnan, 2014).

Other than that, hydrothermal method is a common method used to synthesize TiO_2 thin films. Hydrothermal techniques can be performed in a closed system at a higher autogenous pressure and can directly produce the crystalline structure without further annealing processes. In addition, the hydrothermal process is also useful to produce fine particles with unique morphology and unusual properties (Wu *et al.*, 2008; Meng *et al.*, 2014). The hydrothermal route becomes more auspicious for their potential efficacy in the preparation of the active TiO_2 layer in the devices. It is inexpensive, has high processing speed and easy to control all processing parameters (Dongale *et al.*, 2014). The morphology of TiO_2 thin films was shown in AFM micrograph deposited by hydrothermal route (**Fig. 2a**). It is evident that the deposited TiO_2 thin film is uniform and contained highly dense cubical crystallites. The micrograph shows the agglomerated grainy structure (Dongale *et al.*, 2014). **Fig. 2b** shows TEM images of TiO_2 thin films via hydrothermal method to further investigate the morphology and structure. It can be seen that the prepared TiO_2 nanocrystals have prismatic shapes (Zhao *et al.*, 2013) which both **Fig. 2a** and **Fig. 2b** have the similar shapes. The diameter of the TiO_2 particles depends strongly on the different hydrothermal temperatures. Besides that, when the temperature increases, the particle size and the pore diameter also increases. On the contrary, the surface area of the TiO_2 thin film correspondingly decreases with the rise in temperature (Huang *et al.*, 2006).

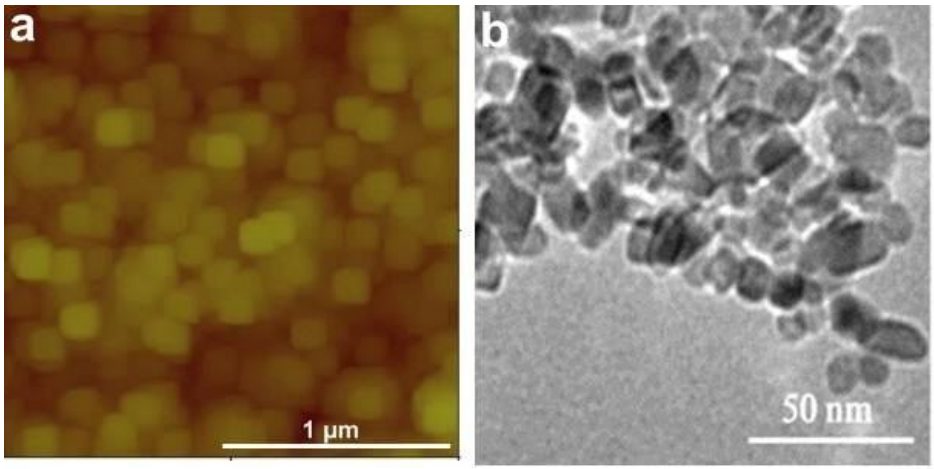

Fig. 2. a) AFM image of TiO_2 thin film grown by hydrothermal route (Dongale *et al.*, 2014) b) TEM image of TiO_2 nanocrystals after heat treatment at 500 °C for 1 h (Zhao *et al.*, 2013).

Recently, single-source precursors (SSPs) provide an alternative synthetic route for the deposition of metal sulfide thin film by AACVD, is attracting more attention because of its obvious advantage such as excellent film uniformity, high deposition rates, control over material composition and phase, conformal coverage on complex geometries, controllability of film microstructures, low-cost and scalability (Hussain *et al.*, 2012). Generally with AACVD process and after decomposition, organic residual and hydroxyl groups will still remain on the top of the films surface and their presence is inevitable. This will give serious effect on the luminescence of rare earth ions. Indeed, when optically excited, the as-deposited films exhibit strong broad band emission in the visible range related to the organic groups, which dominates largely the rare earth emission. Hence, post annealing treatment is indispensable to overcome this problem and eliminate these organic and hydroxyl groups which are entrapped in the films after deposition (Elleuch *et al.*, 2013). The microscopic morphology of the thin films was observed using AFM and FESEM. **Fig. 3a** shows an image of the TiO_2 compact layer. Meanwhile, **Fig. 3b** is TiO_2 deposited for 90 min, using AACVD. The film appears pyramidal with a very compact structure, showing its potential as a blocking layer in the DSSC application (Lim *et al.*, 2014).

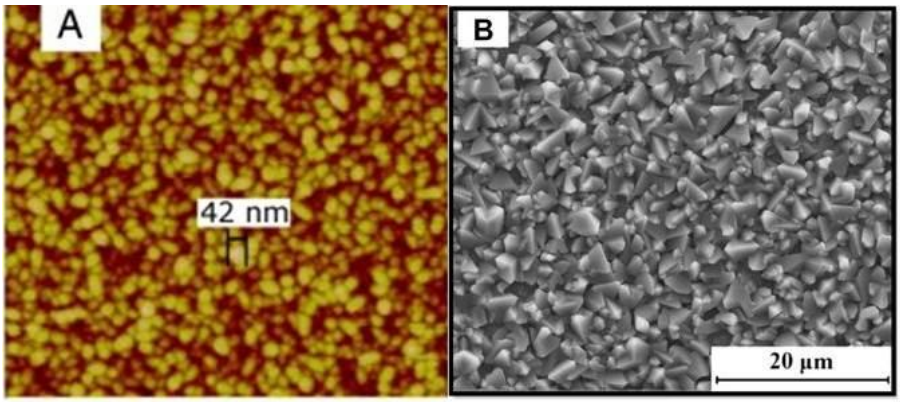

Fig. 3 a) AFM images of TiO_2 film (Chua *et al.*, 2013). b) FESEM images of compact TiO_2 (Lim *et al.*, 2014).

2.5.2 ZnO Working Electrode

Several other semiconductor materials have been developed to substitute TiO_2. For example, zinc oxide (ZnO) has been considered as a promising candidate, as it exhibits the higher electron mobility than TiO_2 (Li *et al.*, 2010). ZnO has been extensively studied as a photoanode due to its high electron mobility (Han *et al.*, 2014) and good resistance to photocorrosion. Moreover, defects induced low intensity absorption in visible region can be exploited to convert ZnO into a good solar light absorber (Shi *et al.*, 2011). ZnO is an n-type wide-band gap semiconductor material with an approximate bandgap of 3.37 eV. Because of its unique properties, ZnO is extensively studied. Low-dimensional ZnO nanocrystals can be formed with stable chemical and thermal properties (Li *et al.*, 2014). However, the power conversion efficiency attained through ZnO based DSSC is very low, when compared with TiO_2 based DSSC. The reason is, due to the dissolution of ZnO thin film in an acidic dye solution followed by the formation of Zn^{2+}/dye complexes, the light interaction and dye stability is affected (Parthiban *et al.*, 2015). A ZnO thin films can be produced using many methods, including sol-gel method and sputtering.

The sol–gel method is relatively easy, simple, and cost-effective for mass production (Maldonado *et al.*, 2010; Li *et al.*, 2014). The SEM images of ZnO thin films are shown in **Fig. 4**. It can be seen that the thin films consist of inhomogeneous and spherical-like shape and hexagonal close-packed structure (Li *et al.*, 2014) nanoparticles and mean grain size of the thin films increase with increasing annealing temperature (Lv *et al.*, 2011). The dense grains was exhibited and a few sharp columns were observed on the surface of the ZnO film via sol-gel method. This may due to the reunion and growth of grains during the annealing process (Xian *et al.*, 2013).

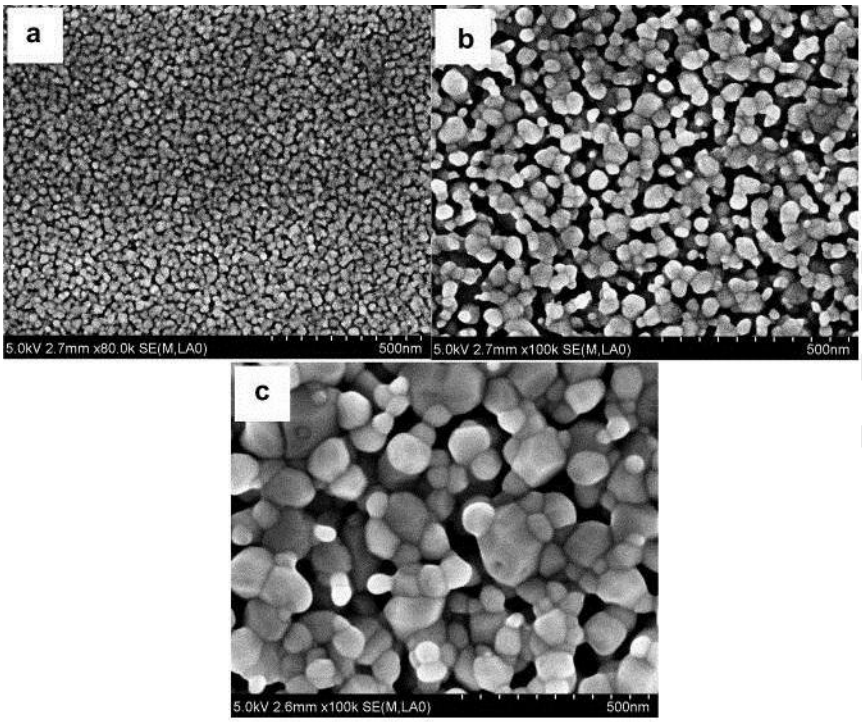

Fig. 4. SEM images of ZnO thin films annealed at (a) 400 °C, (b) 600 °C, and (c) 800 °C (Lv *et al.*, 2011).

Another method that has been used for producing ZnO thin films is sputtering. Reactive sputtering deposition has shown more advantages of controlling the preferred crystalline orientation, growing at relatively low temperature, good interfacial adhesion to the substrate, and high packing density of the grown film (Zhang *et al.*, 2010). AFM images of ZnO thin film are shown in **Fig. 5a**, which showed the uniform surface morphology of the films using sputtering method (Saha *et al.*, 2014). **Fig. 5b** shows FE-SEM top-views of the ZnO film. It shows relatively small individual grains (Zhang *et al.*, 2010). However, there are few types of sputtering methods. One of the examples is rf sputtering. ZnO thin films are deposited in pure Ar and mixed Ar and N_2 gas ambient at various substrate temperatures by rf sputtering ZnO targets. The deposition in pure Ar ambient leads to polycrystalline ZnO thin films. However, the presence of N_2 in the deposition ambient promotes the formation of aligned nanorods at temperatures above 300 °C. ZnO films with aligned nanorods deposited at 500 °C exhibit significantly enhanced photoelectrochemical response, compared to polycrystalline ZnO thin films grown at the same temperature.

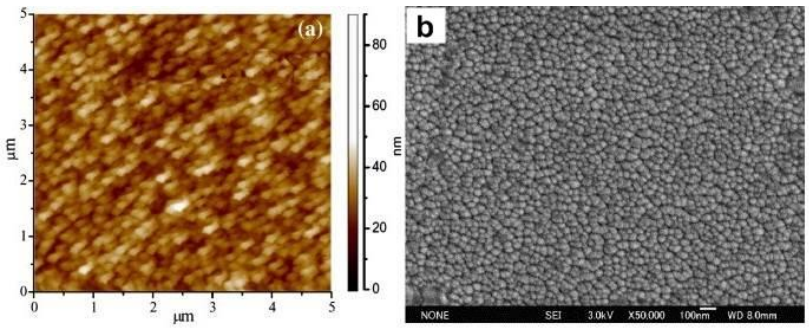

Fig. 5. a) AFM of ZnO film (Saha *et al.*, 2014) b) SEM images of ZnO film deposited at the mixture of Ar:O_2 of 6:4 (Zhang *et al.*, 2010)

2.6 Modification of Working Electrodes for DSSC Application

Each electrode material has its own limitations. Research efforts have been primarily focused on addressing these limitations and achieving better photoelectrodes (Wang *et al.*, 2014). Therefore, chemical modification of semiconductors could increase the performance of DSSC. The recombination of photogenerated electron-hole pairs during charge transfer is a key factors influence the photocatalytic performance. Promoting the separation of photogenerated electrons and holes have gained much attention from researchers (Xu *et al.*, 2014). Several surface modifications have been done on the metal oxide surface, example rGO-TiO_2, ZnO-TiO_2 working electrode and so on. The electrode performance is illustrated by J–V curves under AM 1.5 condition shown in **Fig. 6**. It is observed that a proper amount of the rGO in the rGO–TiO_2 photoanode enhances the energy conversion efficiency of the DSSCs. With 0.75 wt.% rGO, the photoelectric performs the best in this experimental setting with a conversion efficiency of 7.89%, an increase of 30.2% as compared to pure TiO_2-based DSSC (Ding *et al.*, 2015). This is due to the graphene–TiO_2 composites having a good contact between graphene sheets and TiO_2 nanoparticles, which facilitates the electron transfer from TiO_2 to graphene (Zhu *et al.*, 2014). This increase of photocurrent is attributed to the effect of graphene, 2D charge transfer bridges, leading to the improved photogenerated electron transfer ability and reduced charge recombination (Ge *et al.*, 2014; Zhu *et al.*, 2014).

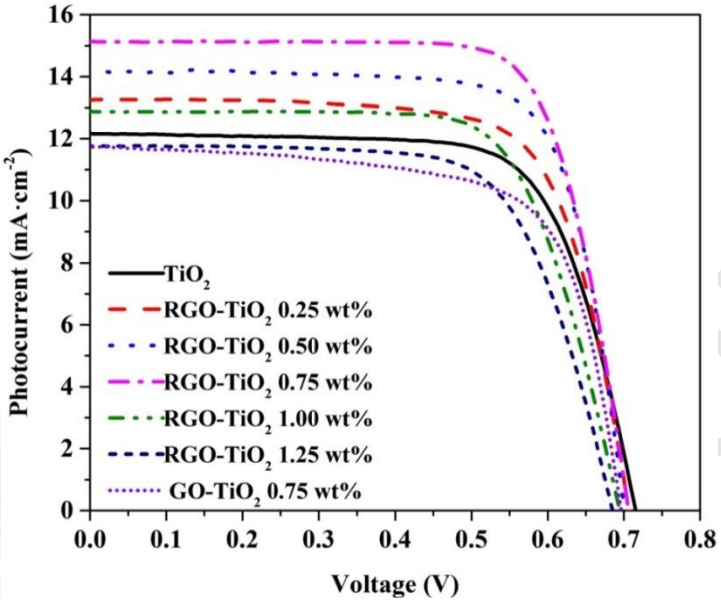

Fig. 6. J–V curves of DSSC with varying amount of rGO/GO (Ding *et al.*, 2015).

For Zn-TiO_2, the efficiency of DSSC is enhancing than TiO_2 (**Fig. 7**). The recombination of the photogenerated carriers is effectively suppressed, leading to an improvement of the electron lifetime and increase of the photocurrent (Guo *et al.*, 2013). The enhancement in charge separation efficiency was contributed to the Schottky barriers formed at the interface between Zn nanoparticles and TiO_2. The Zn nanoparticles acted as sinks for photogenerated charge carriers, and promote interfacial charge-transfer processes in the composite systems (He *et al.*, 2012). In addition, ZnO nanoparticles are attached to the hollow TiO_2 nanofiber surface simultaneously, which improves the electrons transfer rate and light scattering, and suppresses electrons recombination. The highly porous ZnO-TiO_2 surface is beneficial for dye absorbance (Li *et al.*, 2014).

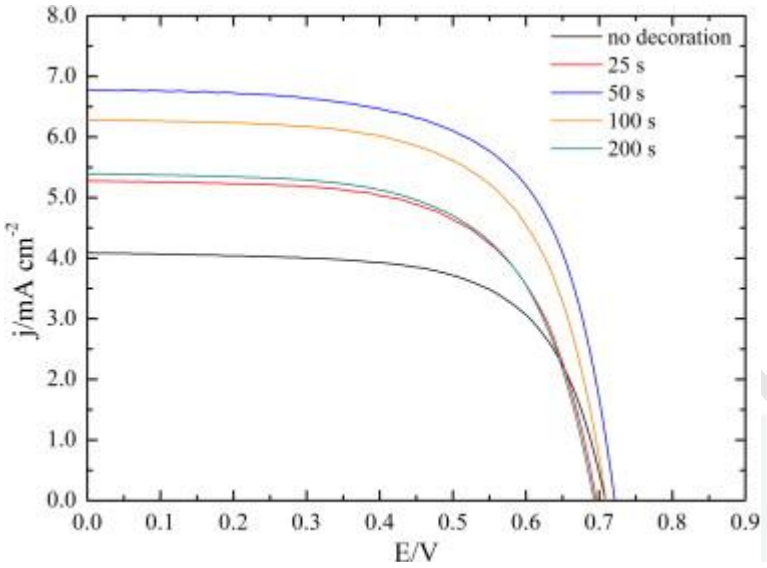

Fig. 7. Photocurrent density–voltage characteristics of DSSCs with as-prepared TiO_2 NTs and ZnO/TiO_2 NTs with different ZnO electrodeposition times under AM 1.5 illumination (Lee *et al.*, 2013).

Zinc oxide has been considered as a promising candidate for DSSCs due to its carrier mobility and direct band gap (3.2 eV), and the position of the conduction band (Habibi *et al.*, 2013). The DSSCs that are based on one-dimensional (1D) ZnO nanostructures exhibit significant advantages so that these nanostructures can provide a passageway for the migration of electrons to the substrate. However, the efficiency of the DSSCs that are based on 1D ZnO nanowires is still at a relatively low level (Zhu *et al.*, 2013). Another key factor in limiting the efficiency of DSSCs based on 1D ZnO nanostructures is the charge recombination at the interface between the ZnO photoelectrode and electrolyte. For suppressing the charge recombination in ZnO dye-sensitized cells, lots of efforts have been made by means of coating the ZnO nanostructures with a conformal metal oxide shell to form a core–shell configuration, such as TiO_2, Al_2O_3, MgO, SnO_2 and so on (Zhou *et al.*, 2014).

Based from Zhou et al.'s study, it is reported the introduction of the SnO_2 layer on the ZnO working electrodes resulted in a more than 39% enhancement of the power conversion efficiency from 2.87% to 4.71% (**Fig. 8**). The SnO_2 layer increased both the open circuit voltage and FF due to the suppressed recombination. SnO_2 could act as a sink for the photogenerated electrons because the conduction band (CB) position of ZnO is higher than that of SnO_2. This charge transfer will increase the spatial separation of injected electrons and oxidized dyes/redox couple, and thus enhance the efficiency of the corresponding DSSCs (Li *et al.*, 2011).

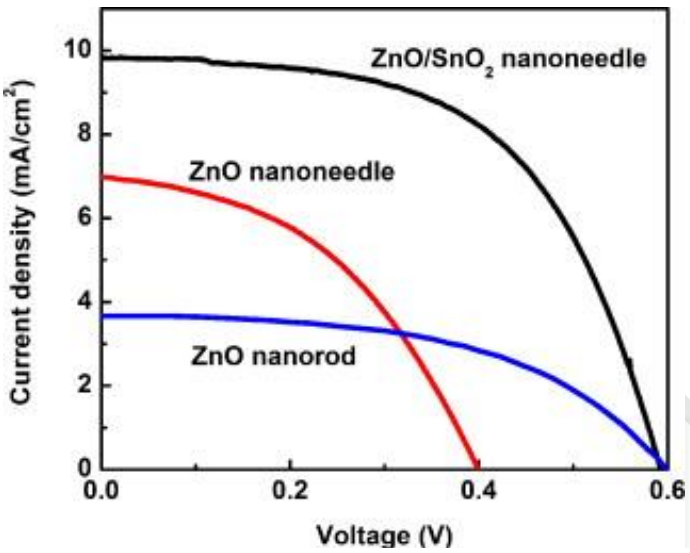

Fig. 8. The compared photocurrent–voltage (*J–V)* characteristics of the cells based on the bare ZnO nanorod, ZnO and ZnO/SnO_2 nanoneedle arrays (Zhou *et al.*, 2014).

Other than that, using metallic nanoparticles such as Ag in solar cells facilitates improving the efficiency of the cell performance because of the enhanced optical absorption and scattering spectrum. So far, this approach has been used in different solar cell structures to modify their performance (Eskandari and Ahmadi, 2015). Ag metal films, which have the highest conductivity of all metals has been already used for ITO-based multilayer for lower resistance, good transparent conducting electrode (Sahu *et al.*, 2006). Based from **Fig. 9**, it is evident that the J_{sc} of all Ag modified ZnO based DSSCs are larger than that of bare ZnO based DSSCs, since the Ag nanoparticles enhance the absorption and charge separation. There is also increasing in the V_{oc} (Tripathi *et al.*, 2015). Other than that, the rough surface of ZnO coated with Ag can be effective in light entrapment for DSSC application and will be beneficial for the enhancement of the photocatalytic activity (Bechambi *et al.*).

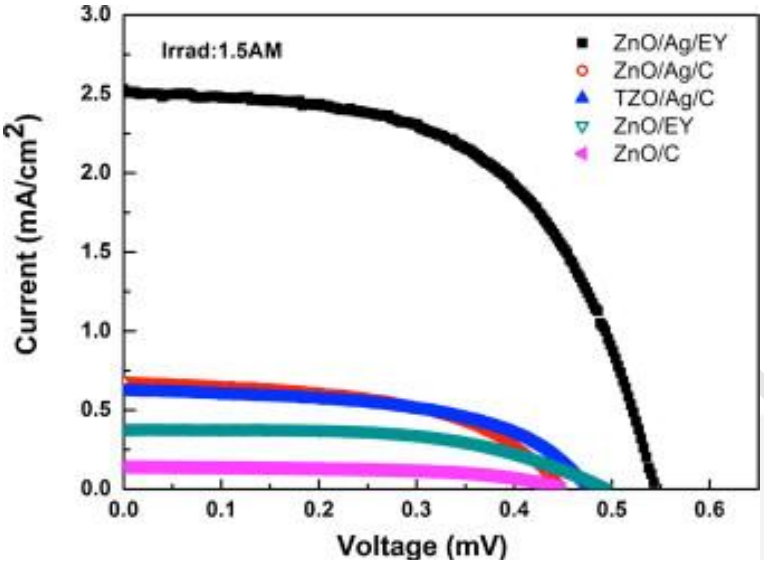

Fig. 9. I-V curve of the dye sensitized solar cells (Tripathi *et al.*, 2015).

2.7 Platinum (Pt)-free Counter Electrodes for DSSC Application

In DSSC, Pt counter electrode has been widely used. A Pt film coated on transparent conducting oxide (TCO) glass substrates is employed as counter electrode (CE) because of its excellent catalytic ability to reduce the triiodide into iodide. However, the commercial viability of Pt as counter electrode has been limited because of (i) its high cost and limited flexibility, (ii) corrosion of the Pt in the presence of small traces of water in the electrolyte, (iii) high temperature processing, and (iv) dissolution of Pt films and formation of PtI_4 (Veerender *et al.*, 2012).

To address these issues, a great deal of research is oriented towards the development of Pt-free counter electrodes such as conducting polymer. Conducting polymers have been studied most intensively due to their easy synthesis, high conductivity, environmental stability, cost effectiveness and unique electrochemical redox properties (Saranya *et al.*, 2015). Conducting polymers such as polyaniline (PANI) and polypyrrole (PPy) as counter electrode have drawn special attention in DSSC.

Among the conducting polymers, polyaniline (PANI) is an excellent one with more advantages, such as its light weight, mechanical flexibility, and low cost (Al-bahrani *et al.*, 2014). Furthermore, PANI film with a certain thickness is found to be excellent transparency in the visible region, which allows fabricating transparent bifacial DSCs with rear-illuminated power conversion efficiency (Peng *et al.*, 2013). Moreover, it has a unique reversible doping/dedoping mechanism, in which protonation by the acid–base reaction leads to an internal redox reaction and conversion from an insulating PANI emeraldine base (PANI-EB) into a conducting PANI emeraldine salt (PANI-ES) (Lee *et al.*, 2013). Additional doping should enhance the conductivity of various electronic forms of PANI, which is of particular interest with regard to

photovoltaic systems. Based from (Ćirić-Marjanović, 2013)'s reviewed study, doping PANI with metal such as Au, Pt, Pd, Ag, Cu and Ni nanoparticles not only retained the original respective intrinsic performances, but also exhibited coadjuvant effect that is beneficial for improving the properties of PANI matrix in composites. Besides PANI/ metal nanoparticles also increased the electrocatalytic and electroanalytical properties. Other than that, doping PANI with nonmetal composites such as carbon nanotube (CNT) and graphene has showed low charge transfer resistance to I_3^-/I^- at the counter electrode/electrolyte of DSSCs and improved the photovoltaic performance of PANI/CNT or PANI/graphene composite to replace Pt counter electrode (Al-bahrani *et al.*, 2014).

As a well known conducting polymer, polypyrrole (PPy) has attracted more and more research interests as a potential candidate for platinized counter electrode because of its facile synthesis, high catalytic activity and considerable environmental stability (Bu *et al.*, 2013). Same goes like PANI, doping Ppy with metal nanostructures such as Pt, Au, Ag, Cu, and Pd seek attention of researchers because of its unique optical and catalytic properties (Jeon *et al.*, 2011; Ghani *et al.*, 2015). Besides, it made the morphologies of counter electrode more porous, which are a few nanometers in size, are easily accessible for the I_3^- ion diffusion. It can be envisaged that the well-distribute metal nanostructures can act as bridges for facilitating electron conductivity, as well as catalysts for enhancing charge transfer between CE surface and electrolytes (Ghani *et al.*, 2015). Moreover, doping Ppy with carbon materials such as carbon nanotubes and graphene also exhibit a higher efficiency and photocurrent because of their fast electron-transport architecture, which also possess an electrocatalytic activity for the I_3^- reduction in the electrolyte (Peng *et al.*, 2011). Besides, the unique nanostructure including large active surface area and network like structure along with large interconnected interstitial volume guaranteed fast mass transport for the electrolyte, and enabled Ppy/carbon materials counter electrode to speed up the reduction of triiodide to iodide (Yue *et al.*, 2014).

2.8 Electrochemistry of DSSC Application

Dye sensitized solar cells (DSSCs) is one of the most promising photovoltaic technologies that have been developed in the last 20 years by virtue of their impressive power conversion efficiency (PCE), low manufacturing cost and long term stability (Sharma *et al.*, 2013). The DSSC has four components: photo-anode, dye, electrolyte and counter-electrode.

Potential sweep methods are widely employed for the study of electrochemical systems. They consist of scanning a specific region of potential while measuring the current response resulting from the electron transfer to or from chemical species involved in the electrochemical reaction (Tamburri *et al.*, 2011). In order to study the electrochemical performances of the activity of reduction I_3^- ions, linear cyclic voltammetry has been used (Yang *et al.*, 2011). The redox reactions involving the I_2/I^- couple include the two sub-reactions listed below:

$$3I_2 + 2e^- \longleftrightarrow 2I_3^- \quad \textbf{(1)}$$

$$I_3^- + 2e^- \longleftrightarrow 3I^- \quad \textbf{(2)}$$

When a dye molecule absorbs light, it excites electrons in the highest occupied molecular orbital to the lowest unoccupied molecular orbital. The excited dye molecule injects an electron into the conducting band of the TiO_2 film. The oxidized dye is restored by electron donation from the reducing ions in the electrolyte, usually an organic solvent containing a redox system. The donated electron is in turn regenerated by the reduction of conjugated ions in the electrolytes. The circuit is completed by electron migration through an external load (Lee *et al.*, 2010).

The photovoltaic properties of the fabricated solar cells were determined by illuminating under solar simulator (Pavithra *et al.*, 2015). Photocurrent-voltage (I-V) curve gained from the analyses of photovoltaic properties, some important photovoltaic parameters for the DSSC can be obtained, such as: (1) the open-circuit voltage, V_{oc}; (2) the short circuit photocurrent density, J_{sc}; (3) the fill factor (FF); and (4) the cell's overall energy conversion efficiency (η). The cell's fill factor can be estimated by according to **Eq. (3)**:

$$FF = \frac{\text{Vmax Jmax}}{\text{Voc Joc}} \quad \textbf{(3)}$$

where V_{max} and J_{max} are the voltage and the current density, respectively, for the maximum power output. Taking into account the ff parameters, the energy conversion efficiency can be calculated as follows (Yang *et al.*, 2011), **Eq. (4)**:

$$\eta\,(\%) = \frac{\text{Voc Jsc FF}}{\text{Is}} \text{x } 100 \quad \textbf{(4)}$$

Electrochemical impedance spectroscopy (EIS) was used in order to better study the electron transport behavior (Shan *et al.*, 2014). The Nyquist plot from EIS, mainly consists of two semicircles from high to low frequency, which is respectively ascribed to the charge-transfer resistance at the interface of the counter electrode–electrolyte (R_{pt}) and the charge-transfer resistance occurring at the working electrode-dye-electrolyte interface (R_{ct}) (Sharma *et al.*, 2013).

CHAPTER 3

MATERIALS AND METHODOLOGY

3.1 Materials

Graphite flakes were purchased from Ashbury Inc. Sulfuric acid (H_2SO_4, 98%), potassium permanganate ($KMnO_4$, 99.9%), hydrogen peroxide (H_2O_2, 30%), silver nitrate ($AgNO_3$, 99.7%) and hydrochloric acid (HCl) were purchased from Systerm, Malaysia. Titanium isopropoxide (TTIP, 98%) and pyrrole were purchased from Acros Organics. Sodium hydroxide (NaOH), and zinc chloride ($ZnCl_2$) were purchased from, Merck, Malaysia. Indium tin oxide (ITO) conducting glass slides (7 Ωsq^{-1}) were commercially supplied by Xin Yan Technology Limited, China. Deionized water was used throughout the experiment. X-ray diffraction patterns were recorded using a Philips X'Pert diffractometer with Cu Kα radiation (λ = 1.5406 Å). The morphology of the TiO_2-rGO thin film was studied using an EI Nova NanoSEM 400 field emission scanning microscope.

3.2 Methods

The following flow chart is a summary of methods used to produce a Pt-free DSSC. Detailed experimental methods are described in the subsequent subtopics.

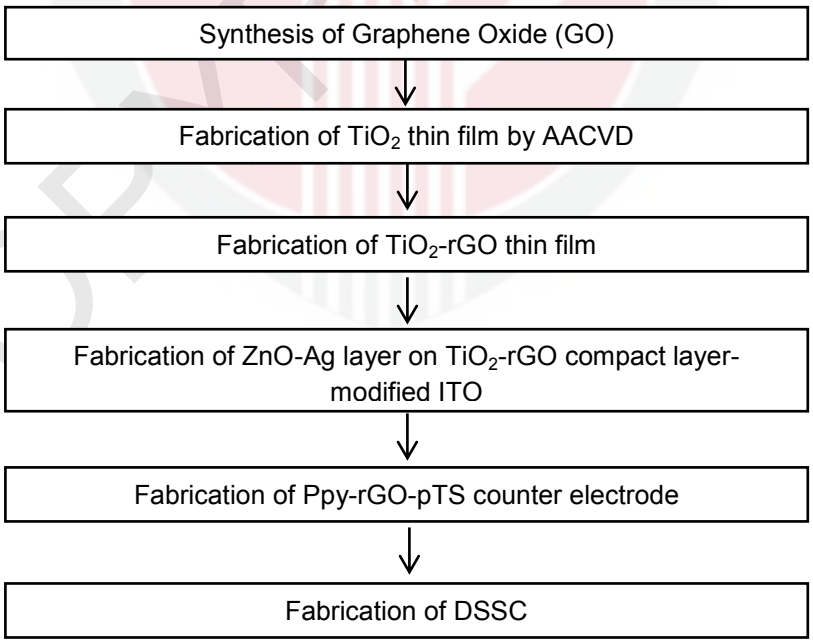

3.2.1 Synthesis of Graphene Oxide (GO)

Graphene oxide (GO) was synthesized using simplified Hummer`s method. Graphite oxide was obtained by oxidation of 3 g of graphite flakes with H_2SO_4:H_3PO_4 (360:40 mL) and 18 g of $KMnO_4$. The mixture was stirred for 3 days using a magnetic stirrer to ensure complete oxidation of graphite. During the oxidation, the color of the mixture changed from dark purplish green to dark brown. To stop the oxidation process, H_2O_2 solution was added and the color of the mixture changed to bright yellow, indicating high oxidation level of graphite. The graphite oxide formed was washed with 1 M of HCl aqueous solution and repeatedly with deionized water until a pH of 4 - 5 was achieved. The washing process was carried out using a simple decantation of the supernatant using centrifugation technique. During the washing process with deionized water, the graphite oxide experienced exfoliation, which resulted in the thickening of the GO solution, forming GO solution. The concentration of the GO solution was 4.8 mg/ml.

3.2.2 Fabrication of TiO_2 thin film by AACVD

TiO_2 thin film was fabricated on the ITO glass substrates (1 cm x 1.5 cm) by an in-house AACVD assembly. The ITO glass was ultrasonically cleaned before use in acetone, NaOH solution and deionized water. 3 mL of the TTIP was dissolved in 50 mL of toluene in a round-bottom flask. Air at a flow rate of 300 mL/min was used as the carrier, and the flow rate was controlled by a flow meter. The aerosol was formed by keeping the flask in a water bath above the piezoelectric modulator of an ultrasonic humidifier (PIFCO ultrasonic humidifier). TTIP aerosol droplets generated was transferred into the hot wall zone of the reactor by the carrier gas, and the deposition was conducted for a period of 30 min. The exhaust from the reactor was vented directly into the extraction system of the fume upboard. The aerosol line was closed toward the end of the experiment and argon gas was allowed to flow. Then, as the prepared TiO_2 thin film was then cooled and stored in air at dark condition.

3.2.3 Fabrication of TiO_2-rGO thin film

Deposition of GO (prepared by simplifying Hummer's method) with different concentration (0.2, 0.4, 0.6, 0.8 and 1.0 mg/mL) on the surface of AACVD-prepared TiO_2 thin film was carried out by dip-coating method. The TiO_2-GO thin film was let in the furnace at 150 ºC and argon gas was allowed to flow for 15 min for the reduction process. The prepared thin films were labelled as TiO_2-0.2rGO, TiO_2-0.4rGO, TiO_2-0.6rGO, TiO_2-0.8rGO and TiO_2-1.0rGO. The sample that had been coated with GO but did not undergo a reduction process was labelled as TiO_2-0.8GO.

3.2.4 Fabrication of ZnO-Ag layer on TiO_2-rGO compact layer-modified ITO

The ZnO-Ag nanocomposite was synthesized using a microwave synthesis technique. 50 ml of deionized water was used to prepare 0.1 M NaOH. Then, 0.1 M of ZnCl and 0.008 M $AgNO_3$ solution were added one at a time into the alkaline solution while stirring. The solution was transferred to a 100-ml Duran

bottle and heated using a microwave oven for 30 min. The bottle was open to the atmosphere. The solution was allowed to cool to room temperature and the precipitate (nanocomposite) was separated from the solution using a centrifuge. The nanocomposite was washed several times with distilled water to remove the ions. In order to compare the efficiency of the DSSC, a ZnO nanocomposite was also prepared using the same method.

3.2.5 Fabrication of Ppy-rGO-pTS counter electrode

The Ppy-rGO-pTS nanocomposite films were fabricated using a catalyst-assisted in-situ electrochemical polymerization method. Briefly, a pyrrole (0.1 M), 2 ml of GO (1 mg/mL), NapTS (1.0 M), and $FeCl_3$ (0.1 M) were mixed in a electrochemical cell and then vigorously stirred for 5 min in order to obtain PPy nanoparticles in the solution. Following the formation of the PPy nanoparticles, the Ppy-rGO-pTS nanocomposite film was deposited at a constant applied potential of +0.8 V using a potentiostat-galvanostat (VersaSTAT 3 electrochemical analyzers from Princeton Applied Research) at room temperature with a 100-s deposition time. For the electrodeposition experiments, indium tin oxide, graphite, and saturated calomel electrodes were used as the working, counter, and reference electrodes, respectively. The as-synthesized counter electrode was denoted as Ppy-rGO-1.0pTS.

3.2.6 Fabrication of DSSC

The prepared film was immersed in an ethanol solution of 0.3 mM N_3 (Ruthenizer 535-bisTBA, Solaronix) dye for 24 h. After sensitization, the film was washed with ethanol. The dye-absorbed electrode was assembled into a sandwich-type cell with a counter electrode (platinum-sputtered ITO glass and polypyrole-graphene oxide film). The counter electrode and dye-sensitized TiO_2-rGO-ZnO-Ag working electrode were clamped firmly together, and a redox electrolyte (Iodolyte Z-100, Solaronix) solution was introduced into the system by capillary action. An active area of 0.5 cm^2 was used to measure the cell performance.

3.3 Characterizations

3.3.1 X-ray Diffraction (XRD)

The crystal phases were characterized by using XRD. Phase identification was performed by XRD using a Philips X'pert system which was equipped with a diffracted –beam graphite monochromator. Scans were conducted using CuKα radiation (1.5406 Å) and a scanning range of 0 to 80 degrees with a scanning rate of 2.0 degrees per minute and a step size of 0.02 degrees.

3.3.2 Field Emission Scanning Electron Microscopy (FESEM)

FESEM was carried out to observe the surface morphology of the TiO_2-rGO thin film by using field emission scanning electron microscope, FEI Quanta 400 F. FESEM magnification was fixed at magnification of 150 000x.

3.3.3 Electrochemistry

The electrochemical characterizations like cyclic voltammetry (CV) and chronoamperometry (CA) were performed with a potentiostat (PAR-VersaSTAT 3). All these voltammetric experiments were done using a conventional three-electrode cell which indium tin oxide (ITO) and platinum wire served as the working electrode (WE) and counter electrode (CE) respectively. The reference electrode (RE) is silver-silver ion (Ag/Ag^{+}).

3.3.4 Contact Angle Measurement

The contact angle measurement was carried out using a contact angle meter (Kwowa Drop Master DMs - 401) to study the surface property of the electrode after modification of the electrode.

3.3.5 DSSC Conversion Efficiency Measurement

The photovoltaic performance of the DSSC was recorded using the VersaSTAT 3 electrochemical analyzer from Princeton Applied Research, under 150-W xenon arc lamp simulated solar illumination, with the use of an AM 1.5G filter. The intensity of the illumination, measured using a fiber optic spectrometer (Avaspec-2048), was 20 mW/cm^2.

CHAPTER 4

RESULTS AND DISCUSSIONS

4.1 Photoelectrochemistry Water Splitting

4.1.1 XRD analysis

Fig. 10 shows X-ray diffraction patterns of AACVD produced TiO_2 and TiO_2-rGO thin film. The XRD pattern of TiO_2 clearly shows the presence of anatase, brookite and mixtures of TiO_2 polymorphs. The anatase peaks are at 25.2º, 48.0º and 55.0º which can be indexed to the (101), (200) and (211) plane and it is good agreement with JCPDS card No. 01-071-1168. Since brookite peak is located at 30.3º that can be indexed to (211) plane (JCPDS card No. 01-076-1937) and mixtures of TiO_2 polymorphs at peaks of 35.2º and 50.7º are indexed to (402) and (203) plane (JCPDS No. 00-046-1237). Meanwhile, the TiO_2-rGO indicates only the presence of anatase TiO_2 at the peak of 25.2º and 48.0º. The brookite and mixtures of TiO_2 polymorphs did not showed any diffraction due to coating of graphene sheet on the TiO_2 surface. The (002) peak of rGO at 25.0º is overlapped with the (101) peak of anatase TiO_2, which originates from the stacked graphene sheets in TiO_2–rGO composite (Nagaraju *et al.*, 2013; Ullah *et al.*, 2014).

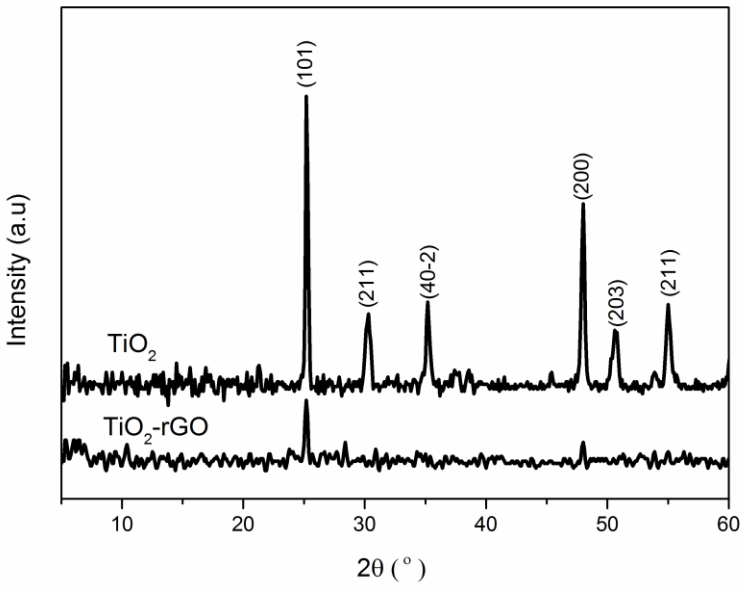

Fig. 10. XRD patterns of TiO_2 thin film and TiO_2-rGO thin film.

4.1.2 Morphological studies

FESEM images of the TiO_2-rGO composite thin film deposited from precursor showed a smooth and compact film morphology with homogeneously dispersed particles. The TiO_2-rGO thin film image (**Fig. 11a**) provides a direct observation on surface morphology of the pure TiO_2 film, from which one can see that TiO_2 particles are spread on glass substrate uniformly and the film processes a flat and crack-free surface structure (Wang *et al.*, 2012). The circled area in **Fig. 11a** is magnified as shown in **Fig. 11b**. The image is clearly seen that the wrinkly film on reduced graphene oxide sheet lays a top the spherical particles, following the contour of the particles (**Fig. 11b**). **Fig. 11b** shows the image of the TiO_2-rGO thin film after being subjected to 1000 cycles of cyclic voltammogram. The image is also seen a rGO sheet coated on the top of the round shape particle. It shows that after went through 1000 cycles of cyclic voltammogram, the morphology of the nanocomposite is still remain the same and rGO is strongly adhered to TiO_2.

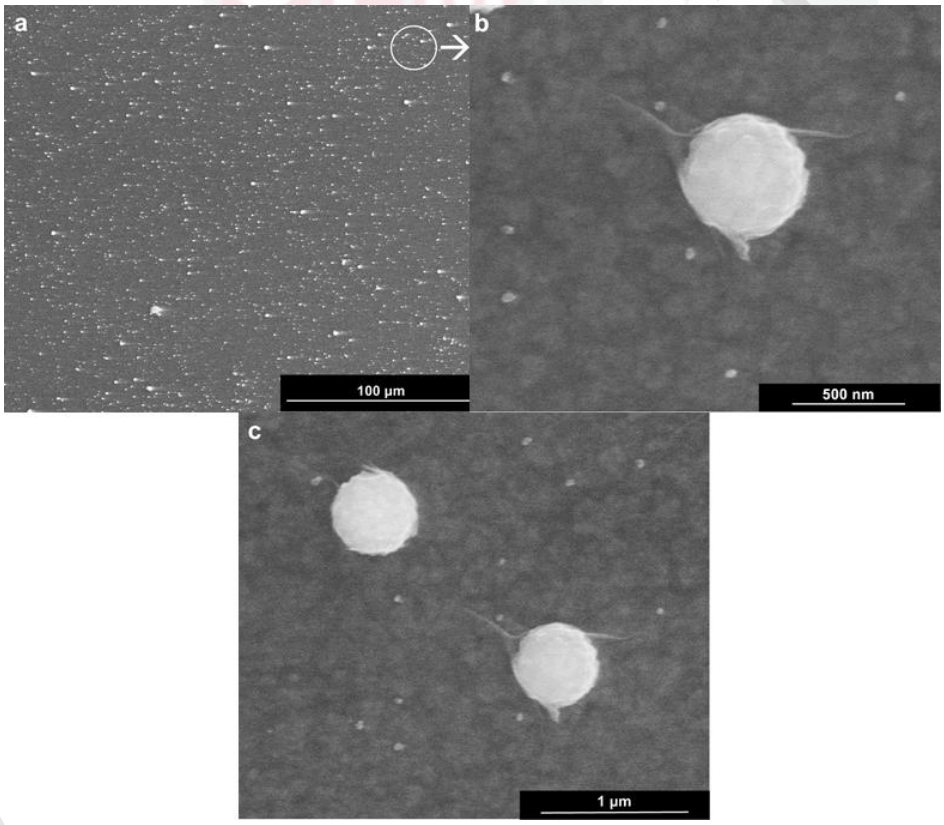

Fig. 11. FESEM images of (a) TiO_2-rGO thin film. (b) magnified TiO_2-rGO. (c) TiO_2-rGO thin film after gone through 1000 cycles of cyclic voltammogram.

4.1.3. Electrochemical studies

Linear sweep voltammetry (LSV) was conducted from +1.0 V to -1.0V under the halogen light irradiation. If the photoresponses occur on the negative side of the potential, this represents p-type semiconductor. As the potential sweeps to the negative direction, cathodic photocurrents are observed is a p-type substance (Zheng *et al.*, 2012). On the other hand, for n-type semiconductor it will photoresponse on the positive side of potential region. Photocurrent was most obvious at the positive cathodic sweep which is belongs to the n-type (Ing *et al.*, 2011). **Fig. 12** shows TiO_2-rGO responsive on the positive side of the potential and it makes as n-type semiconductor. For typical n-type semiconductor, where the photocurrent originates from the supply of photo-holes to the seminconductor/electrolyte interface during illumination (Nowotny *et al.*, 2010).

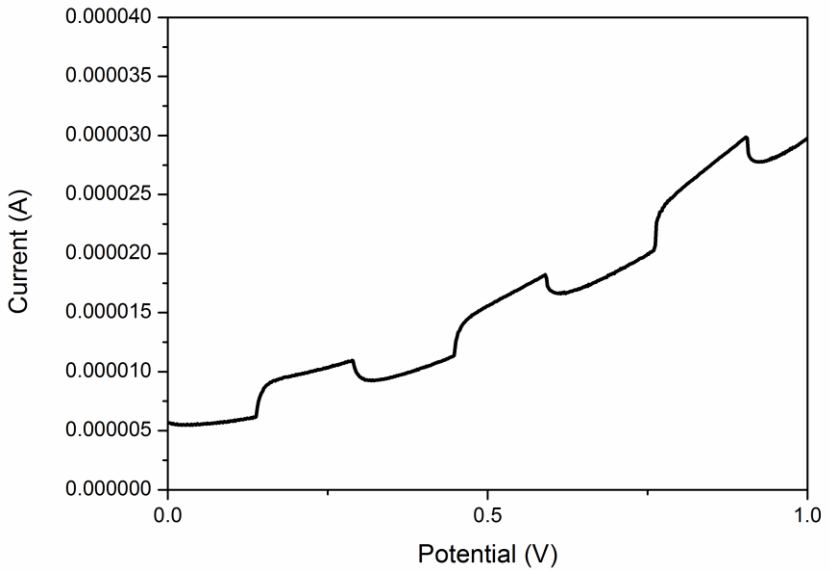

Fig. 12. LSV for n-type TiO_2-rGO thin film determination.

The photosensitive of GO and rGO was studied by mean of linear sweep voltammetry. **Fig. 13** explains better about GO and rGO in the dark and under illumination of light. The graphene sheets acts as an electron transfer channel for reducing the recombination of the photogenerated electron–holes that leads to improved efficiency of the photocatalytic hydrogen production (Nagaraju *et al.*, 2013). The linear sweep voltammograms obtained for GO and rGO confirms the photosensitive to light and it can be seen that the rGO based thin film has distinguishable delivers higher photocurrent than the GO under illumination.

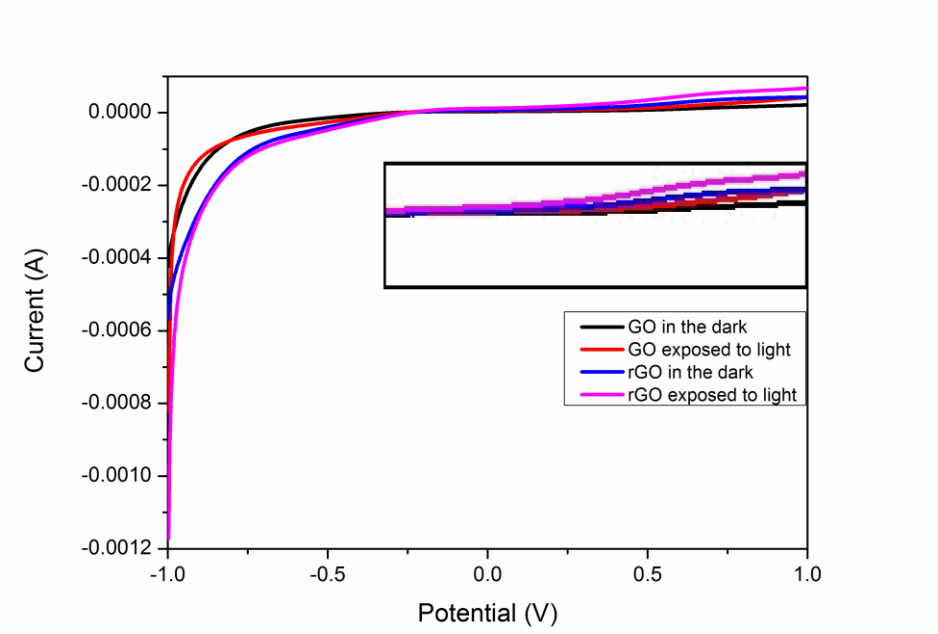

Fig. 13. LSV of GO and rGO in the dark and under light irradiation at scan rate of 0.1 V/s.

The photocurrent, which is sensitive to both electron–hole generation and recombination, has been used to examine the photocurrent activity of the films under illumination of halogen light, the photocurrent versus time profiles were measured. **Fig. 14** showed the influenced of electrolyte on photoelectrochemical performance. It showed the typical real time photocurrent response of the TiO_2-rGO. During the light "on" and "off" conditions at the photoelectrode the rise and fall of the current are very clear. The dark current density was found to be negligible; however, once the light is turned on, a photocurrent is instantaneously generated. In terms of semiconductor physics, when an irradiation provides energy higher than the band gap of TiO_2, the energy excites the electrons from the valence band to the conduction band and leave a hole in valence band (Elghniji *et al.*, 2012). The results show that TiO_2-rGO has an optimum photocurrent for KCl electrolyte, followed by KOH electrolyte, H_2SO_4 electrolyte and Na_2SO_4 electrolyte.

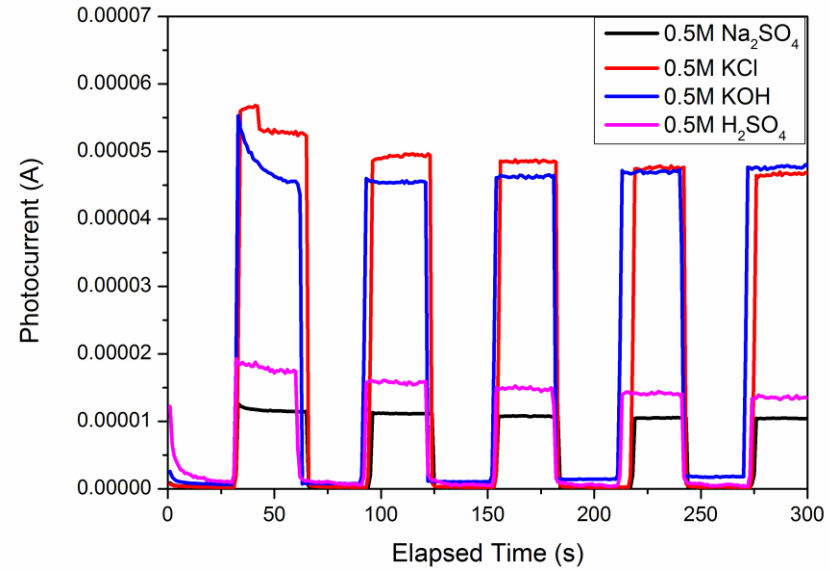

Fig. 14. Photocurrent profile of TiO_2-rGO thin films using different kinds of electrolytes at potential 1.0 V.

Even though KCl electrolyte provides the best photocurrent, Na_2SO_4 electrolyte was used throughout the experiment as it gives a stable CV result even after 1000 cycles (**Fig. 15a**) compared to KCl electrolyte (**Fig. 15b**) after 1000 cycles of CV. Besides, the rate of hydrogen production using TiO_2–rGO under high UV intensity irradiation in the presence of Na_2SO_4 solution exhibited good photocatalytic activity (Nagaraju *et al.*, 2013). Moreover, based from the photocurrent profile (**Fig. 15**) shows Na_2SO_4 gives a stable profile among all electrolyte. It does not have much noise and did not decayed like KCl, KOH and H_2SO_4. So it makes Na_2SO_4 a suitable electrolyte for TiO_2-rGO.

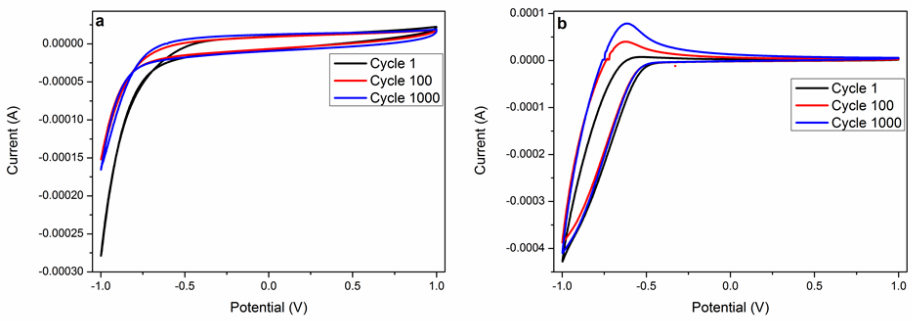

Fig. 15. (a) Cyclic Voltammogram of TiO_2-rGO using Na_2SO_4 as electrolyte. (b) Cyclic Voltammogram of TiO_2-rGO using KCl as electrolyte.

Fig. 16 shows the photocurrent profile of GO, rGO, TiO_2, TiO_2-rGO with different rGO content. It can be observed from the photocurrent profile, graphene coated TiO_2 thin films shows the highest value of photocurrent rather than bare TiO_2 thin film. As a control experiment, the photoresponse of GO and rGO were also measured in the absence of TiO_2 thin film and it showed negligible response. The pure graphene has very low photoresponse, when it combined with TiO_2 showed synergistic photoresponse in the form of composite films (Qin *et al.*, 2014). Among all samples, TiO_2-0.8rGO showed the higher photocurrent which is 80.2 µA followed by TiO_2-1.0rGO (69.0 µA), TiO_2-0.4rGO (41.7 µA), TiO_2-0.2rGO (29.3 µA), TiO_2-0.6rGO (20.1 µA), TiO_2 (12.8 µA) and the lowest photocurrent is TiO_2-0.8GO (5.8 µA). The nature of the TiO_2 photocurrent happened when oxygen molecules of water adsorbed on the TiO_2 surface could react with free electrons, creating negatively charged O_2^- ions. The phenomenon that the photocurrent of TiO_2 dropped abruptly after reaching a maximum value was considered as the process of creating O_2 (Liu *et al.*, 2012). TiO_2 has lower photocurrent than TiO_2-0.8rGO because of the presence of rGO which increase electron transfer efficiency and effectively inhibit the recombination of photoexcited charges. The significantly improved photo-responses confirmed that graphene was a good candidate for the collection and transport of photogenerated charges (Ge *et al.*). It indicated that rGO played an important role in improving the photogenerated carrier separation and enhancing the photocurrent for its excellent electron transport properties (Sun *et al.*, 2014).

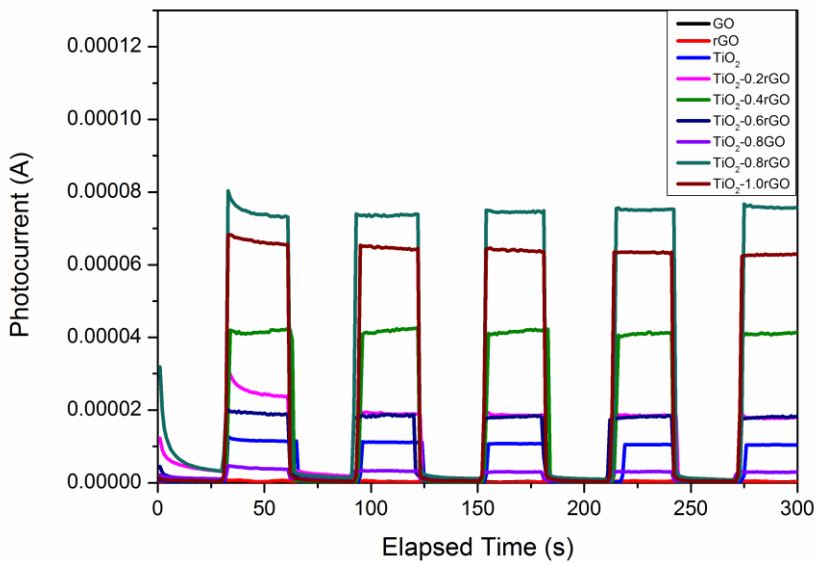

Fig. 16. Photocurrent profile of the as-prepared samples.

The concentration of the GO also plays a role to be a good photoanode. TiO_2-0.8rGO gives the optimum photocurrent among all samples. Therefore, TiO_2-0.8rGO thin film was used for this entire work. For the lower concentration of GO like TiO_2-0.2rGO, TiO_2-0.4rGO and TiO_2-0.6rGO, the photocurrent are

lower than TiO_2-0.8rGO because of limited interface contact between TiO_2 and rGO sheets for photocurrent. Meanwhile, the excessive graphene can act as a kind of recombination center instead of providing an electronic pathway, and the short circuit will happen easily (Liu *et al.*, 2011; Wang *et al.*, 2012) which causes TiO_2-1.0rGO to perform poorly in photocurrent. TiO_2-0.8GO displays poor photocurrent even though it has the same concentration of GO as TiO_2-0.8rGO, implying the importance of the reduction of GO. The presence of oxide functional groups on the basal and the edges of the GO interfere with the electron mobility on the non-conducting GO sheets.

Increasing of applied potential to 0.2, 0.5, 1.0 and 1.5 V, the photocurrent also increased linearly for TiO_2-0.8rGO thin film (**Fig. 17**). The increase in potential increases the rate of charge separation between electrons and holes, which is conducive towards the enhancement of photocurrent and overall photovoltaic conversion efficiency (Zeng *et al.*, 2014). The ability of the as-prepared film to increase in photocurrent in tandem with potential is contributed by the role of rGO as an electron collector, suppressing charge recombination in photoexcited TiO_2 (Ng *et al.*, 2010). This is also presumably due to an increase of GO conductivity by further deoxygenation of GO where oxygen containing functional groups are removed (Min *et al.*, 2012; Ho *et al.*, 2015).

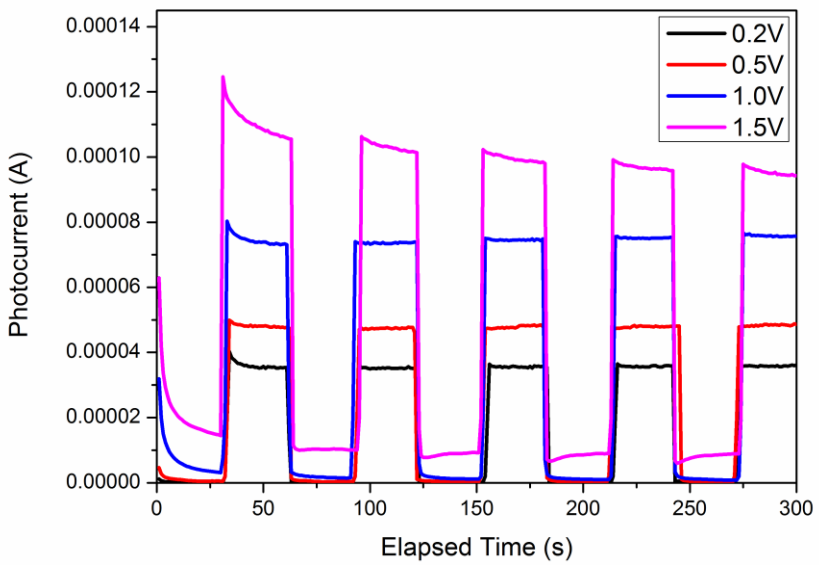

Fig. 17. TiO_2-0.8rGO at potential 0.2 V, 0.5 V, 1.0 V and 1.5 V.

4.2 Dye-sensitized Solar Cell

4.2.1 Working Electrode

4.2.1.1 XRD analysis

Fig. 18 shows the XRD patterns of the ZnO, Zn O-TiO_2-rGO, ZnO-Ag, and ZnO-Ag-TiO_2-rGO, which were used as working electrodes for the as-fabricated DSSCs. The diffraction peaks for ZnO are all consistent with the hexagonal wurtzite structure (JCPDS Card no. 36-1451). The results revealed that the main diffraction peaks were found at 2θ = 31.8°, 34.5°, 36.3°, 47.5°, 56.6°, and 62.9°, which can be attributed to the (002), (100), (101), (102), (110), and (103) planes of the ZnO phase. These peaks are observed in ZnO, ZnO-TiO_2-rGO, ZnO-Ag, and ZnO-Ag-TiO_2-rGO thin films. Meanwhile, after adding Ag to the ZnO, it can be seen in the ZnO-Ag and ZnO-Ag-TiO_2-rGO samples that there are diffraction peaks at 2θ = 38.2° and 44.4°, corresponding to diffraction from planes (111) and (200). The appearance of Ag peaks in the diffraction patterns clearly indicates the formation of crystalline silver clusters in the nanoparticles (JCPDS Card no. 04-0783). A decrease in the peak intensity is generally observed when a doping element with a larger ionic radius than Zn^{2+} is replaced at the substitution sites of the ZnO crystal lattice (Saravanan *et al.*, 2015). The Ag particles preferred to segregate around the grain boundary of ZnO due to the difference in ionic radius between Ag^{+} (1.26 Å) and Zn^{2+} (0.88 Å) (Tripathi *et al.*, 2015). The TiO_2 shows a sharp single phase for the anatase peak of the (101) and (211) planes at 2θ = 25.2° and 55.0° (JCPDS Card no. 21-1272), which can be found in the sample of ZnO-TiO_2-rGO and ZnO-Ag-TiO_2-rGO. The (002) peak of rGO at 25.01° is overlapped by the (101) peak of anatase TiO_2, which originates from the stacked graphene sheets in the TiO_2-rGO composite (Nagaraju *et al.*, 2013; Fa *et al.*, 2014; Ullah *et al.*, 2014).

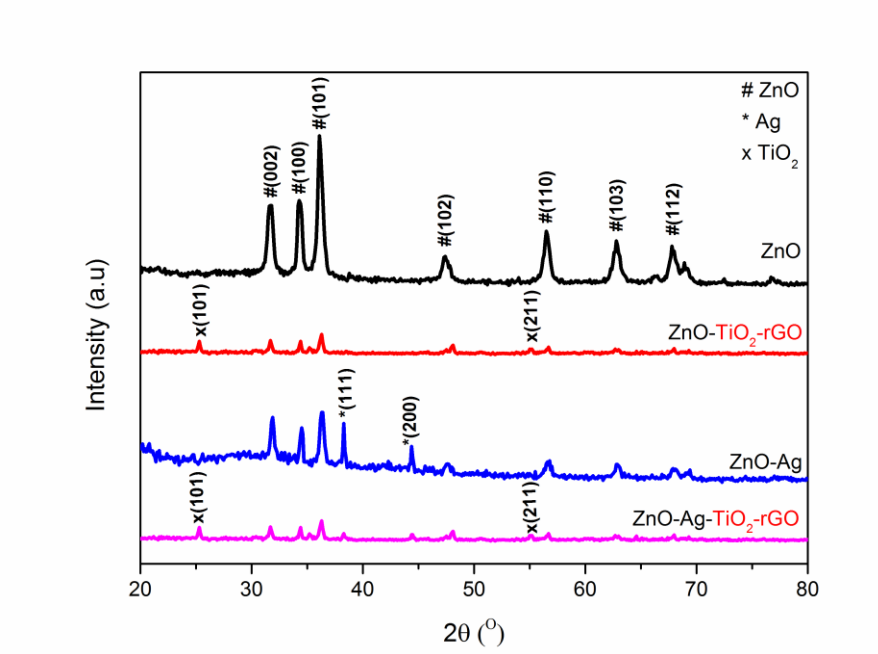

Fig. 18. XRD patterns of as-prepared ZnO, ZnO-TiO_2-rGO, ZnO-Ag and ZnO-Ag-TiO_2-rGO.

4.2.1.2 Morphological studies

Fig. 19 shows FESEM images of the ZnO-TiO_2-rGO and ZnO-Ag-TiO_2-rGO working electrodes. The images only show the active layers of ZnO and ZnO-Ag prepared by the microwave-assisted aqueous solution method using ZnCl, $AgNO_3$, and NaOH because the active layer has covered the whole top of the blocking layer of TiO_2-rGO. The flower shaped structures in **Fig. 19(a)** resulted from the accumulation of several hundreds of sharp-tipped ZnO nanorods, which originated from a single center (Cao *et al.*, 2011). The high degree of porosity of ZnO nanoparticles is clearly displayed in the inset of **Fig. 19(a)**. Such a porous network structure can potentially increase the accessible surface area for enhanced reactant diffusivity, which is highly favorable for photocatalytic applications (Liang *et al.*, 2015) and increased dye absorption for DSSC application (Chang and Kuo, 2010). **Fig. 19(b)** also shows the ZnO-Ag flower-shaped structure, but with the addition of Ag, Ag particles can be obscurely seen attached to the ZnO flower-shaped nanoparticles. This intimate contact makes possible an electronic interaction between the ZnO and Ag and subsequently enhances the charge separation efficiency and photocatalytic activity (Dou *et al.*, 2015).

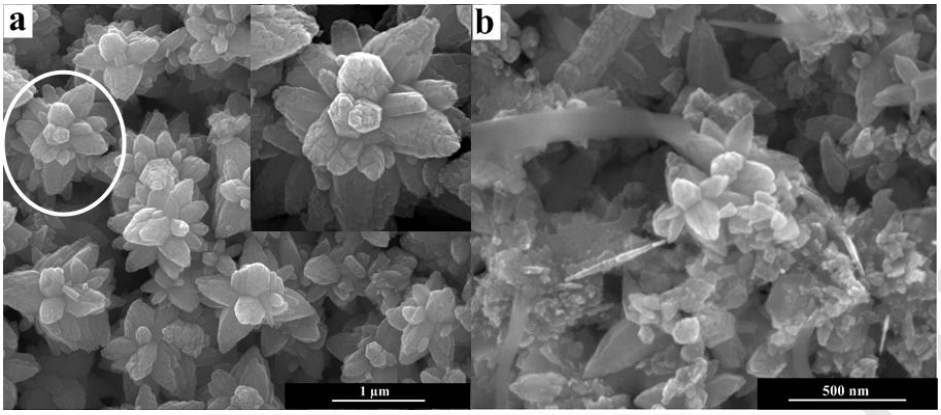

Fig. 19. FESEM images of a) ZnO-TiO_2-rGO and b) ZnO-Ag-TiO_2-rGO working electrodes.

4.2.2 Counter Electrode

4.2.2.1 Morphological studies

Fig. 20(a) depicts Ppy-rGO-1.0pTS at a lower magnification. The large amount of pTS dopant used during the electrodeposition process dictated that the formation of Ppy was in the form of domains or network structures on the rGO sheets (Kumar *et al.*, 2014). The distinguishable components of Ppy and rGO are in contrast to the previously reported Ppy/graphene composite that employed a minimal amount of pTS, in which the composite comprised a thick polymeric Ppy matrix arranged in a layer-by-layer configuration with the graphene sheets (Lim *et al.*, 2013). Moreover, the incorporation of a large-size dopant anion such as pTS into the Ppy-rGO film during electropolymerization resulted in a highly porous film (Rajesh *et al.*, 2004). When observed at a higher magnification, the microspherical grains displayed a typical "cauliflower"-like nodule structure, as shown in **Fig. 20(b)**, which was related to the dopant intercalation within the polymeric chain typically observed for Ppy and pTS synthesized using an electrochemical deposition method (Yoon *et al.*, 1999; Sultana *et al.*, 2012).

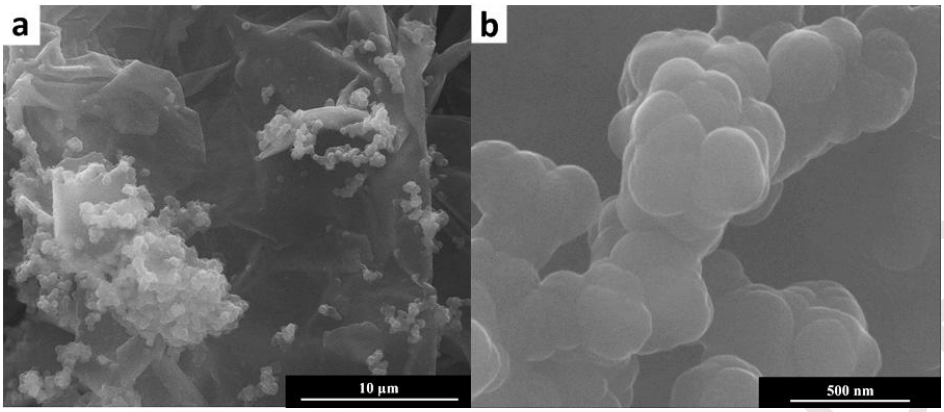

Fig. 20. FESEM images of Ppy-rGO-1.0pTS counter electrode at a a) lower and b) higher magnification.

Fig. 21 presents FESEM images of Ppy-rGO-0.1pTS counter electrodes. **Fig. 28(a)** shows that a high degree of porosity could be of benefit to obtain efficient conductivity, which is crucial to gain high electrocatalytic activity for a counter electrode(Luo *et al.*, 2013; Yue *et al.*, 2014). Meanwhile, **Fig. 21(b)** clearly shows that the Ppy nanoparticles were uniformly distributed on the rGO sheet surface.

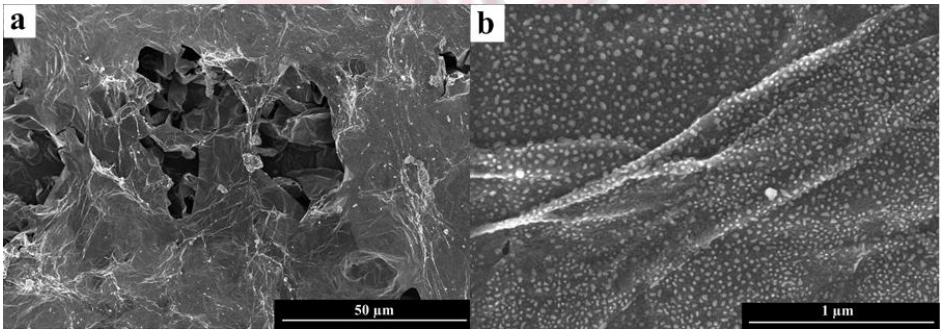

Fig. 21. FESEM images of Ppy-rGO-0.1pTS counter electrode at a) 50 µm and b) 1 µm.

4.2.2.2 Electrochemical studies

Electrochemical impedance spectrocopy (EIS) was conducted to elucidate the electrocatalytic activity of the counter electrode for the as-fabricated DSSCs in relation to the I_3^- reduction reaction by measuring the charge-transfer resistance, which is an important index representing the electrocatalytic performance of a counter electrode. Furthermore, EIS measurements were carried out to compare the conductivity of the Pt, Ppy-rGO-1.0pTS prepared using 1 M of pTS, Ppy-rGO0.1pTS that used 0.1 M of NapTS, and Ppy electrodes. **Fig. 22** shows symmetrical Nyquist plots of the Pt, Ppy-rGO-1.0pTS, Ppy-rGO-0.1pTS (a), and Ppy counter electrodes. The semicircle at the high-frequency range corresponds to the charge-transfer resistance (*Rct*) of

the counter electrode, which describes the catalytic activity for reducing I_3^- The *Rct* for the PPy counter electrode was 31.26 Ω cm^2, indicating that the materials show poor electrocatalytic activity due to the limited conductivity of Ppy. In contrast, the *Rct* value of the Ppy-rGO-0.1pTS electrode was 19.67 Ω cm^2, which was comparable to that of the sputtered Pt electrode (20.7 Ω cm^2), indicating identical intrinsic catalytic activities for the reduction of the I_3^- on the surface of the Ppy-rGO-0.1pTS counter electrode when compared against the Pt counter electrode. We previously reported that the efficiency (η) of a Ppy-rGO-0.1pTS counter electrode-based DSSC was similar to that of a Pt counter electrode-based DSSC (Lim *et al.*, 2014). Ppy-rGO-0.1pTS consisted of PPy nanoparticles decorated on rGO nanosheets (**Fig. 21**). Meanwhile, the *Rct* for the Ppy-rGO-1.0pTS counter electrode was 17.16 Ω cm^2, which was the lowest of all the counter electrodes, suggesting a lower interfacial charge transfer resistance occurring at the interface between the Ppy-rGO counter electrode and I^-/I_3^- electrolyte. This can be attributed to the synergistic catalytic effect, i.e., the improved conductivity and catalytic activity of the Ppy-rGO composite, which enable the electrons to easily transmit across the Ppy-rGO film-ITO interface (Yue *et al.*, 2014). As evidence of the enhanced properties of the Ppy-rGO-1.0pTS counter electrode, common P25 titanium oxide was employed as the working electrode in the fabrication of a DSSC, which displayed a better efficiency (η) than the other counter electrodes (**Fig. 23** and **Table 1**).

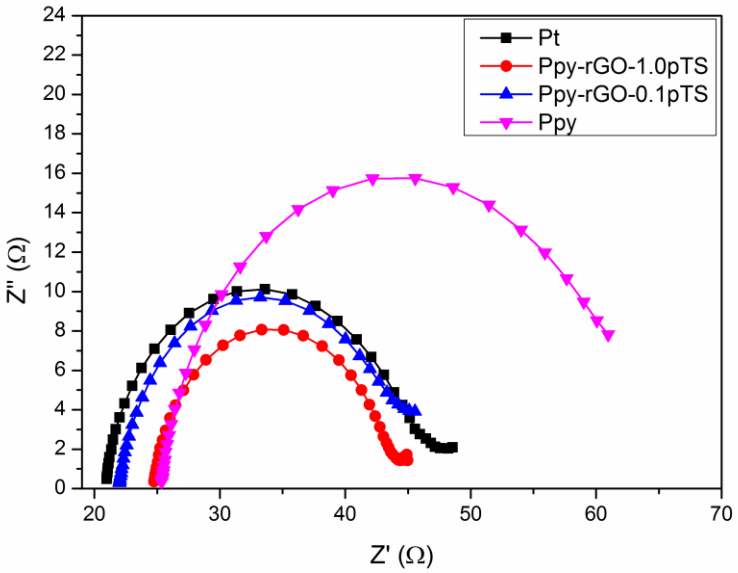

Fig. 22. Nyquist plots of DSSCs using Pt, Ppy-rGO-1.0pTS, Ppy-rGO-0.1pTS and Ppy counter electrodes.

Fig. 23 compares the photovoltaic performances of P25 dye-sensitized solar cells based on a variety of different counter electrodes, including Pt, Ppy-rGO-1.0pTS, Ppy-rGO-0.1pTS, and Ppy counter electrodes. The derived photovoltaic parameters of the short-current density (J_{sc}), open-circuit voltage (V_{oc}), fill factor (FF), and efficiency (η) is summarized in **Table 1**. It can be

seen that the prepared Ppy-rGO-1.0pTS, Ppy-rGO-0.1pTS, and Ppy employed as the counter electrodes in the DSSC device exhibited higher efficiencies of 0.04%, 0.03%, and 0.02%, respectively, compared to the Pt counter electrode (0.002%). The improvements in the FF and J_{sc} values for the DSSC based on the Ppy-rGO-1.0pTS counter electrodes compared to the one fabricated with Ppy can be attributed to its superior electrocatalytic activity and low *R*ct values for I^-/I_3^- redox couples. In addition, the increase in the contact area between the Ppy-rGO counter electrode and electrolyte was responsible for improving the J_{sc} in the DSSC (Yue *et al.*, 2014). The good photovoltaic performance of Ppy-rGO is attributed to the π–π coupling and cation–π coupling interaction between the Ppy and *rGO*, which can take advantage of the synergic effect of the higher electronic conductivity of *rGO* and superior catalytic activity of Ppy. This can reduce the internal series resistance and enhance the FF and J_{sc} values, which in turn lead to higher conversion efficiency (Peng *et al.*, 2011). Comparing the Ppy-rGO1.0pTS and Ppy-rGO0.1pTS counter electrodes, the DSSC with Ppy-rGO-1.0pTS counter electrode presented the highest efficiency. This was attributed to the pTS concentration used in the counter electrode. The higher pTS concentration affected the arrangement of the polypyrrole backbone, which made the polymer more ordered. This ordering in polymer matrix was due to the π–π interaction between the PPy and pTS (Kumar *et al.*, 2014; Vera *et al.*, 2014). It can be ascertained from this that with an increase in pTS doping, the polymers electroactivity was improved. This suggests that the dopant pTS used in the synthesis of Ppy-rGO composites not only offers faster charge transfer kinetics but also improves the stability of the material by preventing overoxidation. Hence, this makes it the best suited candidate for electrodes in electrochemical capacitors (Kumar *et al.*, 2014).

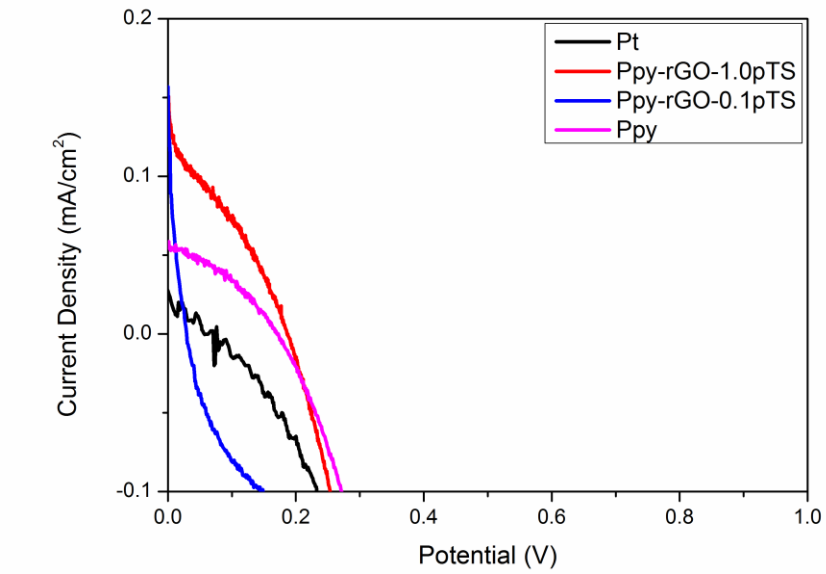

Fig. 23. Photocurrent–voltage characteristics of P25 using Pt, Ppy-rGO-1.0pTS, Ppy-rGO-0.1pTS, and Ppy counter electrodes.

Table 1. Performance parameters of P25 dye-sensitized for Pt, Ppy-rGO-1.0pTS, Ppy-rGO-0.1pTS, and Ppy counter electrodes.

P25	Jsc	Voc	Jmax	Vmax	FF	η(%)
Pt	0.03	0.08	0.003	0.19	0.22	0.002
Ppy-rGO-1.0pTS	0.15	0.19	0.11	0.10	0.27	0.04
Ppy-rGO-0.1pTS	0.15	0.03	0.09	0.07	1.40	0.03
Ppy	0.06	0.17	0.04	0.10	0.38	0.02

Fig. 24 compares the photovoltaic performances of P25, P25-TiO_2, P25-TiO_2-rGO, ZnO, ZnO-TiO_2, ZnO-TiO_2-rGO, ZnO-Ag, ZnO-Ag-TiO_2, and ZnO-Ag-TiO_2-rGO DSSCs with Pt and Ppy-rGO-1.0pTS counter electrodes. The derived photovoltaic parameters of the short-circuit density (J_{sc}), open-circuit voltage (V_{oc}), fill factor (FF), and efficiency (η) for ZnO-Ag-TiO_2-rGO are summarized in **Table 2**. In a comparison of all of the working electrodes used for DSSCs, the Ppy-rGO-1.0pTS counter electrode-based DSSCs achieved significantly higher J_{sc} values than those using the Pt counter electrode. Upon the incorporation of rGO and pTS in PPy, J_{sc} is significantly improved, while FF is slightly increased, resulting in a much improved efficiency (η) of 1.99% compared to that of the Pt counter electrode, which is 0.08%. This might be attributed to the good dispersion of Ppy-rGO complexes, which provide larger active surface areas for I_3^- reduction (He *et al.*, 2014). The counter electrode made up of a highly porous Ppy structure on rGO sheets engendered a large active surface area of the electrode and excellent stability by trapping liquid electrolyte in the micropores (Luo *et al.*, 2013), as depicted in **Fig. 20**. The increased porosity increased the mechanical properties, conductivity, electrochemical relaxation, and ion exchange behaviors of the films (Chengyou and Fenglin, 2006; Sultana *et al.*, 2012). Moreover, introduction of TiO_2-rGO compact layer in DSSC leads to suppress the electron recombination of the ITO and electrolyte, which contributed to a larger contact area with ITO and hence TiO_2-rGO compact layer can provide more effective electron pathways for electron transport (Lim *et al.*, 2015). The increase in the number of electrons at the conduction band of the photoanode, which are eventually transferred to the external circuit, thus significantly increase the DSSC performance.

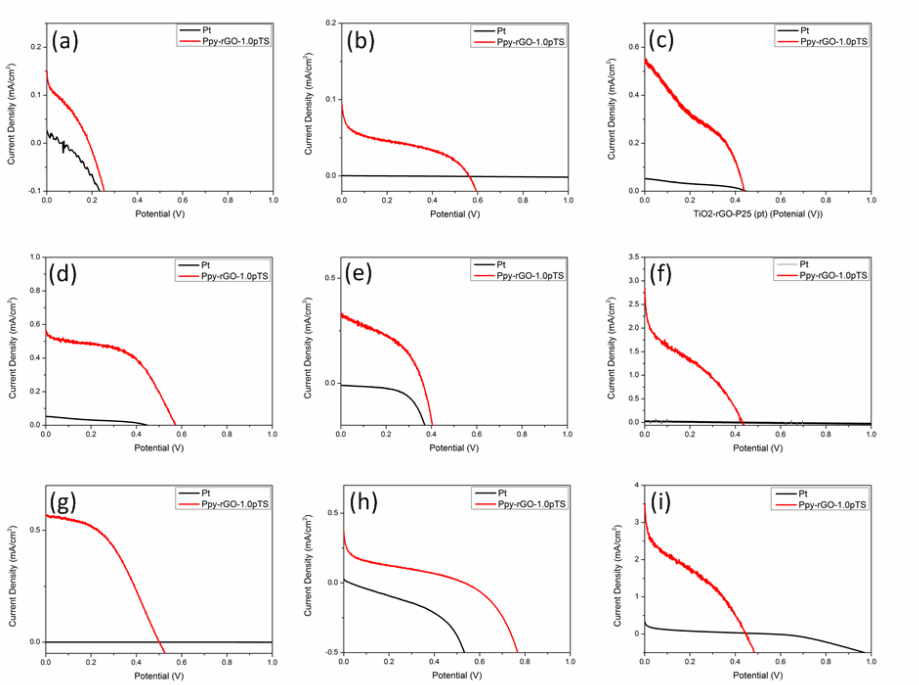

Fig. 24. Photocurrent-voltage characteristics of a) P25 b) P25-TiO_2 c) P25-TiO_2-rGO d) ZnO e) ZnO-TiO_2 f) ZnO-TiO_2-rGO g) ZnO-Ag and h) ZnO-Ag-TiO_2 i) ZnO-Ag-TiO_2-rGO with the Ppy-rGO-1.0pTS (red line) and Pt (black line) counter electrodes under the illumination of AM 1.5 G.

Table 2. Performance parameters of the ZnO-Ag-TiO_2-rGO dye-sensitized for Pt and Ppy-rGO-1.0pTS counter electrodes. Compact layer is labeled in red.

ZnO-Ag-TiO_2-rGO	Jsc	Voc	Jmax	Vmax	FF	η(%)
Pt	0.34	0.52	0.06	0.29	0.09	0.08
Ppy-rGO-1.0pTS	3.51	0.45	1.33	0.30	0.25	1.99

Fig. 25 displays the maximum power densities ($P_{d\text{-}max}$) of the ZnO-Ag-TiO_2-rGO working electrode DSSCs using the Ppy-rGO-1.0pTS counter electrode. The *Jmax* value can be obtained from the photocurrent-voltage graph based on **Equation (5)**:

$$P = J.V \qquad \textbf{(5)}$$

The DSSC with the Ppy-rGO-1.0pTS counter electrode presents the highest short-circuit current density (J_{SC}) of 3.51 mA·cm^{-2},V_{OC} of 0.45 V, and *FF* of 0.25, resulting in a good efficiency of 1.99% compared with that of the one using the sputtered-Pt electrode (0.08%). The enhancement of the *FF* and *Jsc* values for the DSSC based on the Ppy-rGO-1.0pTS counter electrode should be mainly because of its excellent electrochemical catalytic

activity. The enhancement in the *Jsc* values for the DSSC based on the Ppy-rGO-1.0pTS counter electrode is attributed to the increased contact area between the Ppy-rGO counter electrode and electrolyte (Yue *et al.*, 2014). The PPy possesses an excellent electrocatalytic activity for I_3^- reduction, but inferior conductivity; while the rGO can provide high conductivity. Therefore, when PPy is tightly connected to the rGO surface, the PPy can supply active sites to dominantly transform I_3^- to I^-, while simultaneously the rGO will provide a fast electron transport network for the electrolyte (Yue *et al.*, 2014; Yue *et al.*, 2014). Moreover, a planar anion such as pTS induces a charge in the Ppy-rGO molecular configuration, which results in increased electrical conductivity (Rajesh *et al.*, 2004; Jamadade *et al.*, 2011).

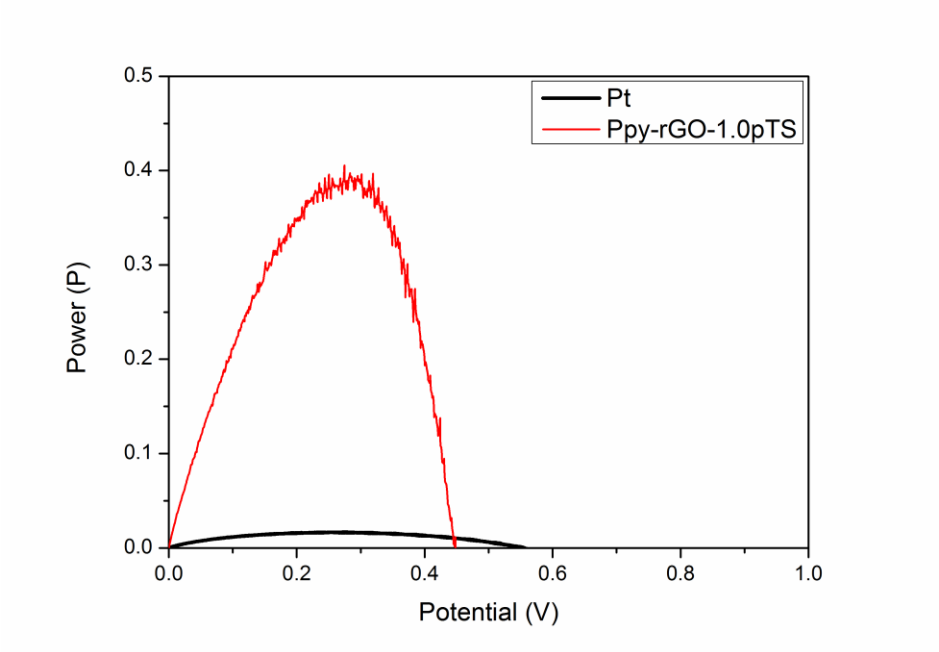

Fig. 25. Plot of power and maximum photovoltage (Vmax) for ZnO-Ag-TiO_2-rGO using Ppy-rGO-1.0pTS and Pt counter electrodes.

4.2.2.3 Contact Angle Measurement

To further characterize the identity of the Ppy-rGO-1.0pTS, **Fig. 26** shows contact angle photographs of the Pt and Ppy-rGO-1.0pTS counter electrodes. The Pt counter electrode (**Fig. 26(a)**) showed a minimum contact angle of 91.2°, which was attributed to its hydrophobicity property (Hu *et al.*, 2012). In comparison, the Ppy-rGO-1.0pTS counter electrode (**Fig. 26(b)**) exhibited a much smaller contact angle of 80.0°, indicating good hydrophilicity. GO is easily solubilized in water because of its hydrophilic functional groups. However, it somehow has a low electronic conductivity caused by the breakdown of the delocalization of π electrons (Park *et al.*, 2014). The conductivity is fairly, but not completely, recovered by reducing GO to rGO, which is extremely hydrophobic (Moozarm Nia *et al.*, 2015). The incorporation of Ppy and rGO solved the hydrophobicity problem of rGO, which apparently

make the counter electrode hydrophilic because Ppy has a hydrophilic property (Liu *et al.*, 2013). The hydrophilic Ppy-rGO-1.0pTS counter electrode gave rise to the efficient extractions of electrons, from which a higher short-circuit current (J_{sc}) and fill factor (FF) were achieved (Zhu *et al.*, 2012). In addition, the hydrophilic surface was found to have a good electrode-electrolyte interfacial contact in the DSSC application (Mane *et al.*, 2009).

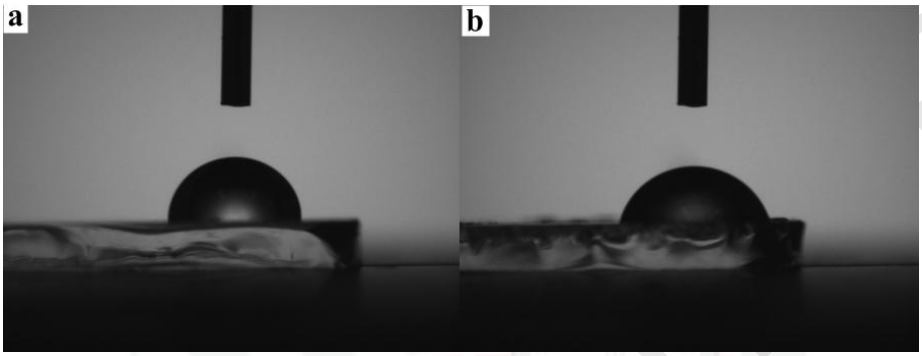

Fig. 26. Contact angles of (a) Pt and (b) Ppy-rGO-1.0pTS counter electrodes.

4.2.2.4 DSSC Conversion Efficiency Measurement

Photocurrent–voltage curves for the DSSCs based on the thin film electrodes are shown in **Fig. 27**. The estimated performance parameters are summarized in **Table 3**. From the analyses of the J–V curves, some important photovoltaic parameters for the DSSC can be obtained, including (1) the open-circuit voltage, V_{oc}; (2) short circuit photocurrent density, J_{sc}; (3) fill factor (FF); and (4) cell's overall energy conversion efficiency (η). The cell's fill factor can be estimated according to **Equation (6)** (Li *et al.*, 2013):

$$FF = \frac{\text{Vmax Jmax}}{\text{Voc Joc}} \qquad \textbf{(6)}$$

where V_{max} and J_{max} are the voltage and current density, respectively, for the maximum power output. Taking into account the FF parameters, the energy conversion efficiency can be calculated according to **Equation (7)** (Yang *et al.*, 2011):

$$\eta\,(\%) = \frac{\text{Voc Jsc FF}}{\text{Is}} \text{x } 100 \qquad \textbf{(7)}$$

The results indicate that the cell sensitized by ZnO-Ag-TiO_2-rGO showed the highest efficiency, with a J_{sc} of 3.51 mA/cm^2, a V_{oc} of 0.45 V, and an FF of 0.25, corresponding to an overall conversion efficiency of 1.99%. Under similar conditions, cells sensitized by ZnO-Ag-TiO_2, ZnO-TiO_2-rGO, ZnO-TiO_2, P25-TiO_2-rGO, P25-TiO_2, ZnO-Ag, ZnO, and P25 exhibited overall efficiencies of 0.14%, 1.47%, 0.25%, 0.39%, 0.11%, 0.63%, 0.78%, and 0.04% respectively. The higher efficiency of ZnO-Ag-TiO_2-rGO compared to ZnO-TiO_2-rGO occurs

because the conductivity of ZnO is improved with the incorporation of Ag ions. This shows that an appropriate amount of Ag can greatly enhance the separation of electron–hole pairs (Xian *et al.*, 2013). In addition, the formation of ZnO–Ag induced a strong electronic coupling, facilitating the interfacial charge transfer processes from ZnO to Ag and further promoting the separation of photogenerated electron–hole pairs (Hou, 2015). P25-TiO_2-rGO gives a lower efficiency than ZnO-TiO_2-rGO and ZnO-Ag-TiO_2-rGO because an energy barrier is constructed by ZnO on the TiO_2 film. This has the potential level of the CB of ZnO (− 0.15 eV), which is higher than the CB of TiO_2 (− 0.1 eV) (Chou *et al.*, 2012). It could also be because TiO_2 has lower electron mobility than ZnO (Li *et al.*, 2014). Moreover, ZnO nanoplates also serve as a barrier layer to remarkably suppress the back reaction, leading to a higher charge collection efficiency than TiO_2 (Wang *et al.*, 2015). The efficiencies of the ZnO-Ag-TiO_2, ZnO-TiO_2, and P25-TiO_2 working electrodes were far lower than those of the working electrodes of ZnO-Ag-TiO_2-rGO and P25-TiO_2-rGO owing to the presence of rGO, which enhanced the electrochemical performance (Saranya *et al.*) and provided high conductivity (Yue *et al.*, 2014). Meanwhile, for ZnO, ZnO-Ag, and P25 without the TiO_2-rGO compact layer, their efficiencies were significantly lower than those of ZnO, ZnO-Ag, and P25 with the TiO_2-rGO compact layer. A compact layer acted as a blocking layer coating on the ITO glass to reduce charge recombination and obtain high photoelectric conversion efficiency. Usually, a dense TiO_2 thin film is prepared and employed as a compact layer to obstruct the back electron transfer from the ITO to the electrolyte (Sun *et al.*, 2014). Along with the help of the electron-accepting and electron-transporting properties of graphene, this also works as a cocatalyst for the rapid transfer of photogenerated electrons (Wang *et al.*, 2013) in the TiO_2, which could indeed suppress the charge recombination and improve the DSSC activities (Nagaraju *et al.*, 2013).

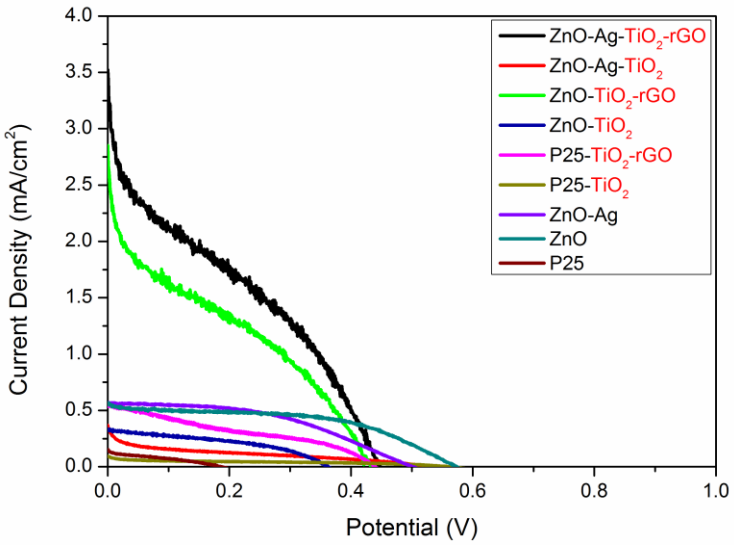

Fig. 27. Photocurrent-voltage characteristics of P25, ZnO, ZnO-Ag, P25-TiO_2, P25-TiO_2-rGO, ZnO-TiO_2, ZnO-TiO_2-rGO, ZnO-Ag-TiO_2 and ZnO-Ag-TiO_2-rGO using Ppy-rGO-1.0pTS counter electrodes. Compact layer is labeled in red.

Table 3. Performance parameters of the dye-sensitized solar cells using Ppy-rGO-1.0pTS counter electrode. Compact layer is labeled in red.

Sample	Jsc	Voc	Jmax	Vmax	FF	η(%)
ZnO-Ag-TiO_2-rGO	3.51	0.45	1.33	0.30	0.25	1.99
ZnO-Ag-TiO_2	0.37	0.53	0.08	0.36	0.15	0.14
ZnO-TiO_2-rGO	2.86	0.43	1.16	0.25	0.24	1.47
ZnO-TiO_2	0.33	0.36	0.20	0.25	0.41	0.25
P25-TiO_2-rGO	0.55	0.44	0.23	0.34	0.32	0.39
P25-TiO_2	0.09	0.56	0.03	0.42	0.44	0.11
ZnO-Ag	0.57	0.50	0.45	0.28	0.44	0.63
ZnO	0.57	0.57	0.42	0.37	0.48	0.78
P25	0.15	0.19	0.07	0.10	0.27	0.04

CHAPTER 5

CONCLUSIONS AND RECOMMENDATIONS

5.1 Conclusions

In summary, TiO_2-rGO thin films were fabricated on ITO substrates as compact blocking layers using AACVD and dip-coating methods. An active layer of ZnO-Ag was introduced on top of the compact layer using a simple dr blade method. It was then applied in a DSSC as a working electrode and could significantly improve both the *Jsc* and *Voc* values of the DSSCs. The TiO_2-rGO blocking layer facilitated electron transfer by preventing electron recombination. It effectively suppressed the back electron transfer, thus improving the open-circuit photovoltage (V_{oc}) and short-circuits photocurrent density (J_{sc}) because of the effect of the blocking layer and the weak energy barrier.

The ZnO-Ag active layer atop the TiO_2-rGO compact layer further promoted the separation of photogenerated electron–hole pairs, which was why the efficiency was higher than those of the ZnO-Ag-TiO_2, ZnO-TiO_2-rGO, ZnO-TiO_2, P25-TiO_2-rGO, P25-TiO_2, ZnO-Ag, ZnO, and P25 working electrodes.

Meanwhile, the highly active and stable in-situ electrochemically deposited Ppy-rGO served as a counter electrode catalyst in the DSSC. The Ppy-rGO counter electrode also showed good catalytic behavior in the DSSC, with respectable values for *Jsc*, *Voc*, and *FF*.

Consequently, a much higher solar conversion efficiency was found for Ppy-rGO-1.0pTS (1.99%) compared to the DSSC based on the sputtered-Pt electrode (0.08%) using the ZnO-Ag-TiO_2-rGO working electrode. This indicated that the incorporation of rGO is an efficient means for enhancing the photovoltaic performance based on the conductive polymer counter electrode. This resulted from (i) altering the hydrophobic surface of rGO to a hydrophilic surface by the introduction of the Ppy nanoparticles on the nanosheets, which consequently improved the interfacial contact between the electrode and electrolyte, and (ii) the presence of pTS, which increased the conductivity. The results foreshadow the development of a new generation of high performance, low-cost DSSCs using a composite counter electrode.

5.2 Recommendations

The following aspects are the improvement for better DSSC that can be included in further studies:

1. Use other natural dyes as photosensitizers that can be obtained in large amount and economically wise such as carotenoids, chlorophylls and anthocyanins. Some of the commercial dyes are synthetic and even require limited heavy metals as active centers what makes recycling more difficult.

2. Antioxidants can be added to protect the pigments from oxidation in DSSC. In addition, antioxidants should also be used to improve the efficiency of the cell.

3. Use positive (*p*)-type semiconductors like nickel(II) oxide (NiO) or copper(I) thiocyanate (CuSCN) that transport positive holes since *n*-type semiconductors like TiO_2 has been widely used.

4. Constitute copper phthalocyanine with the TiO_2-dye complex to increase the efficiency with using Ru based dye N719.

REFERENCES

Abdin, Z., M. A. Alim, R. Saidur, M. R. Islam, W. Rashmi, S. Mekhilef and A. Wadi (2013). "Solar energy harvesting with the application of nanotechnology." Renewable and Sustainable Energy Reviews 26(0): 837-852.

Abdullah, M. H. and M. Rusop (2013). "Multifunctional graded index TiO2 compact layer for performance enhancement in dye sensitized solar cell." Applied Surface Science 284(0): 278-284.

Abdullah, M. H. and M. Rusop (2013). "Novel ITO/arc-TiO2 antireflective conductive substrate for transmittance enhanced properties in dye-sensitized solar cells." Microelectronic Engineering 108(0): 99-105.

Abdullah, M. H. and M. Rusop (2014). "Improved performance of dye-sensitized solar cell with a specially tailored TiO2 compact layer prepared by RF magnetron sputtering." Journal of Alloys and Compounds 600(0): 60-66.

Abdullah, M. H. and M. Rusop (2014). "RF sputtered tri-functional antireflective TiO2 (arc-TiO2) compact layer for performance enhancement in dye-sensitised solar cell." Ceramics International 40(1, Part A): 967-974.

Abergel, D. S. L., V. Apalkov, J. Berashevich, K. Ziegler and T. Chakraborty (2010). "Properties of graphene: a theoretical perspective." Advances in Physics 59(4): 261-482.

Aghigh, A., V. Alizadeh, H. Y. Wong, M. S. Islam, N. Amin and M. Zaman (2015). "Recent advances in utilization of graphene for filtration and desalination of water: A review." Desalination 365(0): 389-397.

Al-bahrani, M. R., X. Xu, W. Ahmad, X. Ren, J. Su, Z. Cheng and Y. Gao (2014). "Highly efficient dye-sensitized solar cell with GNS/MWCNT/PANI as a counter electrode." Materials Research Bulletin 59(0): 272-277.

Ashok, C. H. and K. Venkateswara Rao (2014). "ZnO/TiO2 nanocomposite rods synthesized by microwave-assisted method for humidity sensor application." Superlattices and Microstructures 76(0): 46-54.

Babu, D. D., S. R. Gachumale, S. Anandan and A. V. Adhikari (2015). "New D-π-A type indole based chromogens for DSSC: Design, synthesis and performance studies." Dyes and Pigments 112(0): 183-191.

Bechambi, O., M. Chalbi, W. Najjar and S. Sayadi "Photocatalytic activity of ZnO doped with Ag on the degradation of endocrine

disrupting under UV irradiation and the investigation of its antibacterial activity." Applied Surface Science(0).

Benedetti, J. E., A. A. Corrêa, M. Carmello, L. C. P. Almeida, A. S. Gonçalves and A. F. Nogueira (2012). "Cross-linked gel polymer electrolyte containing multi-wall carbon nanotubes for application in dye-sensitized solar cells." Journal of Power Sources 208(0): 263-270.

Bhande, S. S., D. V. Shinde, K. K. Tehare, S. A. Patil, R. S. Mane, M. Naushad, Z. A. Alothman, K. N. Hui and S. H. Han (2014). "DSSCs synergic effect in thin metal oxide layer-functionalized SnO2 photoanodes." Journal of Photochemistry and Photobiology A: Chemistry 295: 64-69.

Brinker, C. J., G. C. Frye, A. J. Hurd and C. S. Ashley (1991). "Fundamentals of sol-gel dip coating." Thin Solid Films 201(1): 97-108.

Bu, C., Q. Tai, Y. Liu, S. Guo and X. Zhao (2013). "A transparent and stable polypyrrole counter electrode for dye-sensitized solar cell." Journal of Power Sources 221(0): 78-83.

Cao, Y., B. Liu, R. Huang, Z. Xia and S. Ge (2011). "Flash synthesis of flower-like ZnO nanostructures by microwave-induced combustion process." Materials Letters 65(2): 160-163.

Chae, J., D. Y. Kim, S. Kim and M. Kang (2010). "Photovoltaic efficiency on dye-sensitized solar cells (DSSC) assembled using Ga-incorporated TiO2 materials." Journal of Industrial and Engineering Chemistry 16(6): 906-911.

Chang, C. J. and E. H. Kuo (2010). "Light-trapping effects and dye adsorption of ZnO hemisphere-array surface containing growth-hindered nanorods." Colloids and Surfaces A: Physicochemical and Engineering Aspects 363(1–3): 22-29.

Chang, H., C. H. Chen, M. J. Kao, S. H. Chien and C. Y. Chou (2013). "Photoelectrode thin film of dye-sensitized solar cell fabricated by anodizing method and spin coating and electrochemical impedance properties of DSSC." Applied Surface Science 275(0): 252-257.

Chen, L., H. Xie, W. Yu, B. Wang and Z. Wu (2015). "Thermal transport behaviors of suspended graphene sheets with different sizes." International Journal of Thermal Sciences 94(0): 221-227.

Chengyou, J. and Y. Fenglin (2006). "Ion transport and conformational relaxation of a polypyrrole film in aqueous solutions." Sensors and Actuators, B: Chemical 114(2): 737-739.

Cholula-Díaz, J. L., J. Barzola-Quiquia, H. Krautscheid, U. Teschner and P. Esquinazi (2014). "Synthesis and magnetotransport properties

of nanocrystalline graphite prepared by aerosol assisted chemical vapor deposition." Carbon 67(0): 10-16.

Chou, C. S., F. C. Chou and J. Y. Kang (2012). "Preparation of ZnO-coated TiO2 electrodes using dip coating and their applications in dye-sensitized solar cells." Powder Technology 215–216(0): 38-45.

Chua, C. S., O. K. Tan, M. S. Tse and X. Ding (2013). "Photocatalytic activity of tin-doped TiO2 film deposited via aerosol assisted chemical vapor deposition." Thin Solid Films 544(0): 571-575.

Ćirić-Marjanović, G. (2013). "Recent advances in polyaniline composites with metals, metalloids and nonmetals." Synthetic Metals 170(0): 31-56.

Conibeer, G., M. Green, R. Corkish, Y. Cho, E. C. Cho, C. W. Jiang, T. Fangsuwannarak, E. Pink, Y. Huang, T. Puzzer, T. Trupke, B. Richards, A. Shalav and K.-l. Lin (2006). "Silicon nanostructures for third generation photovoltaic solar cells." Thin Solid Films 511–512(0): 654-662.

de Moraes, A. C. M., P. F. Andrade, A. F. de Faria, M. B. Simões, F. C. C. S. Salomão, E. B. Barros, M. d. C. Gonçalves and O. L. Alves (2015). "Fabrication of transparent and ultraviolet shielding composite films based on graphene oxide and cellulose acetate." Carbohydrate Polymers 123(0): 217-227.

Ding, H., S. Zhang, J. T. Chen, X. P. Hu, Z. F. Du, Y. X. Qiu and D. L. Zhao (2015). "Reduction of graphene oxide at room temperature with vitamin C for RGO–TiO2 photoanodes in dye-sensitized solar cell." Thin Solid Films 584: 29-36.

Ding, H., S. Zhang, J. T. Chen, X. P. Hu, Z. F. Du, Y. X. Qiu and D. L. Zhao (2015). "Reduction of graphene oxide at room temperature with vitamin C for RGO–TiO2 photoanodes in dye-sensitized solar cell." Thin Solid Films(0).

Dongale, T. D., S. S. Shinde, R. K. Kamat and K. Y. Rajpure (2014). "Nanostructured TiO2 thin film memristor using hydrothermal process." Journal of Alloys and Compounds 593(0): 267-270.

Dou, P., F. Tan, W. Wang, A. Sarreshteh, X. Qiao, X. Qiu and J. Chen (2015). "One-step microwave-assisted synthesis of Ag/ZnO/graphene nanocomposites with enhanced photocatalytic activity." Journal of Photochemistry and Photobiology A: Chemistry 302(0): 17-22.

Duong, T. T., H. J. Choi, Q. J. He, A. T. Le and S. G. Yoon (2013). "Enhancing the efficiency of dye sensitized solar cells with an SnO2 blocking layer grown by nanocluster deposition." Journal of Alloys and Compounds 561(0): 206-210.

Dupuy, L., S. Haller, J. Rousset, F. Donsanti, J. F. Guillemoles, D. Lincot and F. Decker (2010). "Impedance measurements of nanoporosity in electrodeposited ZnO films for DSSC." Electrochemistry Communications 12(5): 697-699.

Ehsan, M. A., A. A. Tahir, M. Hamid, M. Mazhar, K. G. U. Wijayantha and M. Zeller (2011). "Deposition of iron titanate/titania ceramic composite thin films from a single molecular precursor." Inorganica Chimica Acta 376(1): 189-194.

Elghniji, K., A. Atyaoui, S. Livraghi, L. Bousselmi, E. Giamello and M. Ksibi (2012). "Synthesis and characterization of Fe3+ doped TiO2 nanoparticles and films and their performance for photocurrent response under UV illumination." Journal of Alloys and Compounds 541(0): 421-427.

Elleuch, R., R. Salhi, N. Maalej, J. L. Deschanvres and R. Maalej (2013). "Structural and luminescence correlation of annealed Er-ZnO/Si thin films deposited by AACVD process." Materials Science and Engineering: B 178(17): 1124-1129.

Eskandari, M. and V. Ahmadi (2015). "Treatment Effects of ZnO and Al:ZnO Photoanodes on Short-Circuit Photocurrent and Open-Circuit Photovoltage of Quantum Dot Sensitized Solar Cell Using Ag Nanoparticles." Electrochimica Acta 165(0): 239-246.

Fa, J., L. Hn, Z. Z, H. Nm and P. A (2014). "Titanium dioxide-reduced graphene oxide thin film for photoelectrochemical water splitting." Ceramics International 40(9, Part B): 15159-15165.

Fan, L. Q., G. J. Liu, J. H. Wu, L. Liu, J. M. Lin and Y. L. Wei (2014). "Asymmetric supercapacitor based on graphene oxide/polypyrrole composite and activated carbon electrodes." Electrochimica Acta 137(0): 26-33.

Fang, Y., X. Ai, X. Wang, Q. Wang, J. Huang and T. Wu (2014). "Effect of TiOx compact layer with varied components on the performance of dye-sensitized solar cells." Journal of Alloys and Compounds 594(0): 211-216.

Fang, Y., X. Wang, X. Ai, J. Huang, Q. Wang and T. Wu (2014). "Sputtered TiOx thin film as compact layer for solid-state dye sensitized solar cells." Ceramics International 40(10, Part A): 15941-15949.

Gadipelli, S. and Z. X. Guo (2015). "Graphene-based materials: Synthesis and gas sorption, storage and separation." Progress in Materials Science 69(0): 1-60.

Gao, R., Y. Cui, X. Liu and L. Wang (2014). "Compact TiO2 Film Photoanode for Investigating the Interlayer of Alternating Assembly

Structure in Dye-sensitized Solar Cells." Electrochimica Acta 129(0): 85-92.

Ge, L., Y. Wang, H. Yang, P. Yang, X. Cheng, M. Yan and J. Yu "A photoelectrochemical biosensor using ruthenium complex-reduced graphene oxide hybrid as the photocurrent signal reporter assembled on rhombic TiO2 nanocrystals driven by visible light." Analytica Chimica Acta(0).

Ge, L., Y. Wang, H. Yang, P. Yang, X. Cheng, M. Yan and J. Yu (2014). "A photoelectrochemical biosensor using ruthenium complex-reduced graphene oxide hybrid as the photocurrent signal reporter assembled on rhombic TiO2 nanocrystals driven by visible light." Analytica Chimica Acta 828(0): 27-33.

Gerischer, H., M. E. Michel-Beyerle, F. Rebentrost and H. Tributsch (1968). "Sensitization of charge injection into semiconductors with large band gap." Electrochimica Acta 13(6): 1509-1515.

Ghani, S., R. Sharif, S. Bashir, A. A. Zaidi, M. S. Rafique, A. Ashraf, S. Shahzadi, S. Rafique and A. H. Kamboh (2015). "Polypyrrole thin films decorated with copper nanostructures as counter electrode for dye-sensitized solar cells." Journal of Power Sources 282(0): 416-420.

Guai, G. H., Q. L. Song, Z. S. Lu, C. M. Ng and C. M. Li (2013). "Tailor and functionalize TiO2 compact layer by acid treatment for high performance dye-sensitized solar cell and its enhancement mechanism." Renewable Energy 51(0): 29-35.

Guo, D., J. Wang, C. Cui, P. Li, X. Zhong, F. Wang, S. Yuan, K. Zhang and Y. Zhou (2013). "ZnO@TiO2 core–shell nanorod arrays with enhanced photoelectrochemical performance." Solar Energy 95(0): 237-245.

Habibi, M. H., B. Karimi, M. Zendehdel and M. Habibi (2013). "Fabrication, characterization of two nano-composite CuO–ZnO working electrodes for dye-sensitized solar cell." Spectrochimica Acta Part A: Molecular and Biomolecular Spectroscopy 116(0): 374-380.

Han, W., L. Ren, X. Qi, Y. Liu, X. Wei, Z. Huang and J. Zhong (2014). "Synthesis of CdS/ZnO/graphene composite with high-efficiency photoelectrochemical activities under solar radiation." Applied Surface Science 299(0): 12-18.

Han, Z., Z. Zhao, Z. Du, L. Zhao and X. Cong (2014). "A novel anode material of TiCl4 treatment on Ag/TiO2 in DSSC." Materials Letters 136(0): 424-426.

He, B., Q. Tang, J. Luo, Q. Li, X. Chen and H. Cai (2014). "Rapid charge-transfer in polypyrrole–single wall carbon nanotube complex

counter electrodes: Improved photovoltaic performances of dye-sensitized solar cells." Journal of Power Sources 256(0): 170-177.

He, H., P. Xiao, Y. Zhang, Y. Jia, Y. Yang and Z. Qiao (2012). "Effect of Zn nanoparticles morphology on the photoelectrochemical properties of Zn/TiO2NTs nanocomposites." Journal of Alloys and Compounds 522(0): 63-68.

Ho, C. Y., C. C. Liang and H. W. Wang (2015). "Investigation of low thermal reduction of graphene oxide for dye-sensitized solar cell counter electrode." Colloids and Surfaces A: Physicochemical and Engineering Aspects 481: 222-228.

Hou, X. (2015). "ZnO/Ag heterostructured nanoassemblies: Wet-chemical preparation and improved visible-light photocatalytic performance." Materials Letters 139(0): 201-204.

Hou, X. and K. L. Choy (2006). "Processing and Applications of Aerosol-Assisted Chemical Vapor Deposition." Chemical Vapor Deposition 12(10): 583-596.

Hu, S., J. Hou, L. Xiong, K. Weng, X. Ren and Y. Luo (2012). "Preparation and characterization of hydrophobic Pt–Fe catalysts with enhanced catalytic activities for interface hydrogen isotope separation." Journal of Hazardous Materials 209–210(0): 478-483.

Huang, C. Y., Y. C. Hsu, J. G. Chen, V. Suryanarayanan, K. M. Lee and K. C. Ho (2006). "The effects of hydrothermal temperature and thickness of TiO2 film on the performance of a dye-sensitized solar cell." Solar Energy Materials and Solar Cells 90(15): 2391-2397.

Huang, N., Y. Liu, T. Peng, X. Sun, B. Sebo, Q. Tai, H. Hu, B. Chen, S. S. Guo and X. Zhao (2012). "Synergistic effects of ZnO compact layer and TiCl4 post-treatment for dye-sensitized solar cells." Journal of Power Sources 204(0): 257-264.

Huang, Y. H., J. H. Chen, X. Sun, Z. B. Su, H. T. Xing, S. R. Hu, W. Weng, H. X. Guo, W. B. Wu and Y. S. He (2015). "One-pot hydrothermal synthesis carbon nanocages-reduced graphene oxide composites for simultaneous electrochemical detection of catechol and hydroquinone." Sensors and Actuators B: Chemical 212(0): 165-173.

Hussain, S. T., S. A. Bakar, B. Saima and B. Muhammad (2012). "Low temperature deposition of silver sulfide thin films by AACVD for gas sensor application." Applied Surface Science 258(24): 9610-9616.

Ing, Y. C., Z. Zainal, A. Kassim and W. M. M. Yunus (2011). "Electrochemical Preparation of Bilayer pn Junction of n-CdS/p-P3HT." International Journal of Electrochemical Science 6.

Jamadade, S., S. V. Jadhav and V. Puri (2011). "Electromagnetic reflection, shielding and conductivity of polypyrrole thin film electropolymerized in P-Tulensulfonic acid." Journal of Non-Crystalline Solids 357(3): 1177-1181.

Jana, A., P. P. Das, S. A. Agarkar and P. Sujatha Devi (2014). "A comparative study on the dye sensitized solar cell performance of solution processed ZnO." Solar Energy 102(0): 143-151.

Jang, B. and A. Zhamu (2008). "Processing of nanographene platelets (NGPs) and NGP nanocomposites: a review." Journal of Materials Science 43(15): 5092-5101.

Jeon, S. S., C. Kim, J. Ko and S. S. Im (2011). "Spherical polypyrrole nanoparticles as a highly efficient counter electrode for dye-sensitized solar cells." Journal of Materials Chemistry 21(22): 8146-8151.

Kaveri, S., L. Thirugnanam, M. Dutta, J. Ramasamy and N. Fukata (2013). "Thiourea assisted one-pot easy synthesis of CdS/rGO composite by the wet chemical method: Structural, optical, and photocatalytic properties." Ceramics International 39(8): 9207-9214.

Khan, M., C. Wei, M. Chen, J. Tao, N. Huang, Z. Qi and L. Li (2014). "CTAB-mediated synthesis and characterization of ZnO/Ag core–shell nanocomposites." Journal of Alloys and Compounds 612(0): 306-314.

Kovash Jr, C. S., J. D. Hoefelmeyer and B. A. Logue (2012). "TiO2 compact layers prepared by low temperature colloidal synthesis and deposition for high performance dye-sensitized solar cells." Electrochimica Acta 67(0): 18-23.

Kumar, A., R. K. Singh, H. K. Singh, P. Srivastava and R. Singh (2014). "Enhanced capacitance and stability of p-toluenesulfonate doped polypyrrole/carbon composite for electrode application in electrochemical capacitors." Journal of Power Sources 246(0): 800-807.

Kuo, H. P., C. F. Yang, A. N. Huang, C. T. Wu and W. C. Pan (2014). "Preparation of the working electrode of dye-sensitized solar cells: Effects of screen printing parameters." Journal of the Taiwan Institute of Chemical Engineers 45(5): 2340-2345.

Kwak, B. S., H. Lee and M. Kang (2014). "Synthesis and photoelectric properties of visible sensitive SnS2-linked graphene composites." Chemical Engineering Journal 255(0): 613-622.

Lee, J. C., K. H. Kang, S. K. Kim, K. H. Yoon, I. J. Park and J. Song (2000). "RF sputter deposition of the high-quality intrinsic and n-type ZnO window layers for Cu(In,Ga)Se2-based solar cell applications." Solar Energy Materials and Solar Cells 64(2): 185-195.

Lee, K. M., E. S. Lee, B. Yoo and D. H. Shin (2013). "Synthesis of ZnO-decorated TiO2 nanotubes for dye-sensitized solar cells." Electrochimica Acta 109(0): 181-186.

Lee, Y., J. Chae and M. Kang (2010). "Comparison of the photovoltaic efficiency on DSSC for nanometer sized TiO2 using a conventional sol–gel and solvothermal methods." Journal of Industrial and Engineering Chemistry 16(4): 609-614.

Lee, Y. W., K. Do, T. H. Lee, S. S. Jeon, W. J. Yoon, C. Kim, J. Ko and S. S. Im (2013). "Iodine vapor doped polyaniline nanoparticles counter electrodes for dye-sensitized solar cells." Synthetic Metals 174(0): 6-13.

Lewkowicz, A., A. Synak, B. Grobelna, P. Bojarski, R. Bogdanowicz, J. Karczewski, K. Szczodrowski and M. Behrendt (2014). "Thickness and structure change of titanium(IV) oxide thin films synthesized by the sol–gel spin coating method." Optical Materials 36(10): 1739-1744.

Li, B., L. Luo, T. Xiao, X. Hu, L. Lu, J. Wang and Y. Tang (2011). "Zn2SnO4–SnO2 heterojunction nanocomposites for dye-sensitized solar cells." Journal of Alloys and Compounds 509(5): 2186-2191.

Li, C. F., C. Y. Hsu and Y. Y. Li (2014). "NH3 sensing properties of ZnO thin films prepared via sol–gel method." Journal of Alloys and Compounds 606(0): 27-31.

Li, F., G. Wang, Y. Jiao, J. Li and S. Xie (2014). "Efficiency enhancement of ZnO-based dye-sensitized solar cell by hollow TiO2 nanofibers." Journal of Alloys and Compounds 611(0): 19-23.

Li, H., Z. Xie, Y. Zhang and J. Wang (2010). "The effects of ethyl cellulose on PV performance of DSSC made of nanostructured ZnO pastes." Thin Solid Films 518(24, Supplement): e68-e71.

Li, J., H. Feng, J. Li, Y. Feng, Y. Zhang, J. Jiang and D. Qian (2015). "Fabrication of gold nanoparticles-decorated reduced graphene oxide as a high performance electrochemical sensing platform for the detection of toxicant Sudan I." Electrochimica Acta 167(0): 226-236.

Li, J., J. Li, Q. Chen, J. Bai and B. Zhou (2013). "Converting hazardous organics into clean energy using a solar responsive dual photoelectrode photocatalytic fuel cell." Journal of Hazardous Materials 262(0): 304-310.

Li, M., W. Guo, H. Li, S. Xu, C. Qu and B. Yang (2014). "Synthesis of chemical vapor deposition graphene on tantalum wire for supercapacitor applications." Applied Surface Science 317(0): 1100-1106.

Li, Y., H. Yu, C. Zhang, L. Fu, G. Li, Z. Shao and B. Yi (2013). "Electrodeposition of Ni oxide on TiO2 nanotube arrays for enhancing visible light photoelectrochemical water splitting." Journal of Electroanalytical Chemistry 688(0): 228-231.

Liang, J., G. Zhang, W. Sun and P. Dong (2015). "High efficiency flexible fiber-type dye-sensitized solar cells with multi-working electrodes." Nano Energy 12(0): 501-509.

Liang, S., L. Zhu, G. Gai, Y. Yao, J. Huang, X. Ji, X. Zhou, D. Zhang and P. Zhang (2014). "Synthesis of morphology-controlled ZnO microstructures via a microwave-assisted hydrothermal method and their gas-sensing property." Ultrasonics Sonochemistry 21(4): 1335-1342.

Liang, Y., N. Guo, L. Li, R. Li, G. Ji and S. Gan (2015). "Fabrication of porous 3D flower-like Ag/ZnO heterostructure composites with enhanced photocatalytic performance." Applied Surface Science 332(0): 32-39.

Lim, S. P., N. M. Huang, H. N. Lim and M. Mazhar (2014). "Aerosol assisted chemical vapour deposited (AACVD) of TiO2 thin film as compact layer for dye-sensitised solar cell." Ceramics International 40(6): 8045-8052.

L
im, S. P., A. Pandikumar, N. M. Huang and H. N. Lim (2015). "Reduced graphene oxide–titania nanocomposite-modified photoanode for efficient dye-sensitized solar cells." International Journal of Energy Research 39(6): 812-824.

Lim, S. P., A. Pandikumar, Y. S. Lim, N. M. Huang and H. N. Lim (2014). "In-situ electrochemically deposited polypyrrole nanoparticles incorporated reduced graphene oxide as an efficient counter electrode for platinum-free dye-sensitized solar cells." Sci. Rep. 4.

Lim, Y. S., Y. P. Tan, H. N. Lim, N. M. Huang and W. T. Tan (2013). "Preparation and characterization of polypyrrole/graphene nanocomposite films and their electrochemical performance." Journal of Polymer Research 20(6): 1-10.

Liu, D., P. Yang, X. Yuan, J. Guo and N. Liao (2015). "The defect location effect on thermal conductivity of graphene nanoribbons based on molecular dynamics." Physics Letters A 379(9): 810-814.

Liu, L., F. Zhao, J. Liu and F. Yang (2013). "Preparation of highly conductive cathodic membrane with graphene (oxide)/PPy and the membrane antifouling property in filtrating yeast suspensions in EMBR." Journal of Membrane Science 437(0): 99-107.

Liu, X., L. Pan, T. Lv, G. Zhu, Z. Sun and C. Sun (2011). "Microwave-assisted synthesis of CdS-reduced graphene oxide composites for

photocatalytic reduction of Cr(vi)." Chemical Communications 47(43): 11984-11986.

Liu, Y., S. Wei and W. Gao (2015). "Ag/ZnO heterostructures and their photocatalytic activity under visible light: Effect of reducing medium." Journal of Hazardous Materials 287(0): 59-68.

Liu, Y., C. Xie, J. Li, T. Zou and D. Zeng (2012). "New insights into the relationship between photocatalytic activity and photocurrent of TiO2/WO3 nanocomposite." Applied Catalysis A: General 433–434(0): 81-87.

Lou, Y., S. Yuan, Y. Zhao, P. Hu, Z. Wang, M. Zhang, L. Shi and D. Li (2013). "A simple route for decorating TiO2 nanoparticle over ZnO aggregates dye-sensitized solar cell." Chemical Engineering Journal 229(0): 190-196.

Low, F. W., C. W. Lai and S. B. Abd Hamid (2015). "Easy preparation of ultrathin reduced graphene oxide sheets at a high stirring speed." Ceramics International 41(4): 5798-5806.

Lu, J., H. Wang, S. Dong, F. Wang and Y. Dong (2014). "Effect of Ag shapes and surface compositions on the photocatalytic performance of Ag/ZnO nanorods." Journal of Alloys and Compounds 617(0): 869-876.

Ludin, N. A., A. M. Al-Alwani Mahmoud, A. Bakar Mohamad, A. A. H. Kadhum, K. Sopian and N. S. Abdul Karim (2014). "Review on the development of natural dye photosensitizer for dye-sensitized solar cells." Renewable and Sustainable Energy Reviews 31(0): 386-396.

Luo, J., H. J. Niu, H. I. Wen, W. J. Wu, P. Zhao, C. Wang, X. D. Bai and W. Wang (2013). "Enhancement of the efficiency of dye-sensitized solar cell with multi-wall carbon nanotubes/polypyrrole composite counter electrodes prepared by electrophoresis/electrochemical polymerization." Materials Research Bulletin 48(3): 988-994.

Lv, J., W. Gong, K. Huang, J. Zhu, F. Meng, X. Song and Z. Sun (2011). "Effect of annealing temperature on photocatalytic activity of ZnO thin films prepared by sol–gel method." Superlattices and Microstructures 50(2): 98-106.

Ma, J., J. Liu, Y. Bao, Z. Zhu, X. Wang and J. Zhang (2013). "Synthesis of large-scale uniform mulberry-like ZnO particles with microwave hydrothermal method and its antibacterial property." Ceramics International 39(3): 2803-2810.

Maldonado, A., S. Tirado-Guerra, J. M. Cázares and M. d. l. L. Olvera (2010). "Physical and sensing properties of ZnO:F:Al thin films deposited by sol-gel." Thin Solid Films 518(7): 1815-1820.

Mane, R. S., J. Chang, D. Ham, B. N. Pawar, T. Ganesh, B. W. Cho, J. K. Lee and S.-H. Han (2009). "Dye-sensitized solar cell and electrochemical supercapacitor applications of electrochemically deposited hydrophilic and nanocrystalline tin oxide film electrodes." Current Applied Physics 9(1): 87-91.

Meher, S. R. and L. Balakrishnan (2014). "Sol–gel derived nanocrystalline TiO2 thin films: A promising candidate for self-cleaning smart window applications." Materials Science in Semiconductor Processing 26(0): 251-258.

Meng, H., W. Hou, X. Xu, J. Xu and X. Zhang (2014). "TiO2-loaded activated carbon fiber: Hydrothermal synthesis, adsorption properties and photo catalytic activity under visible light irradiation." Particuology 14(0): 38-43.

Meng, L., H. Chen, C. Li and M. P. dos Santos (2015). "Preparation and characterization of dye-sensitized TiO2 nanorod solar cells." Thin Solid Films 577(0): 103-108.

Menzel, R., D. Ogermann, S. Kupfer, D. Weiß, H. Görls, K. Kleinermanns, L. González and R. Beckert (2012). "4-Methoxy-1,3-thiazole based donor-acceptor dyes: Characterization, X-ray structure, DFT calculations and test as sensitizers for DSSC." Dyes and Pigments 94(3): 512-524.

Min, Y., K. Zhang, L. Chen, Y. Chen and Y. Zhang (2012). "Sonochemical assisted synthesis of a novel TiO2/graphene composite for solar energy conversion." Synthetic Metals 162(9–10): 827-833.

Minami, T., T. Miyata and Y. Nishi (2014). "Cu2O-based heterojunction solar cells with an Al-doped ZnO/oxide semiconductor/thermally oxidized Cu2O sheet structure." Solar Energy 105(0): 206-217.

Moozarm Nia, P., W. P. Meng, F. Lorestani, M. R. Mahmoudian and Y. Alias (2015). "Electrodeposition of copper oxide/polypyrrole/reduced graphene oxide as a nonenzymatic glucose biosensor." Sensors and Actuators B: Chemical 209(0): 100-108.

Nagaraju, G., G. Ebeling, R. V. Gonçalves, S. R. Teixeira, D. E. Weibel and J. Dupont (2013). "Controlled growth of TiO2 and TiO2–RGO composite nanoparticles in ionic liquids for enhanced photocatalytic H2 generation." Journal of Molecular Catalysis A: Chemical 378(0): 213-220.

Ng, Y. H., I. V. Lightcap, K. Goodwin, M. Matsumura and P. V. Kamat (2010). "To What Extent Do Graphene Scaffolds Improve the Photovoltaic and Photocatalytic Response of TiO2 Nanostructured Films?" The Journal of Physical Chemistry Letters 1(15): 2222-2227.

Nishi, Y., T. Miyata and T. Minami (2013). "The impact of heterojunction formation temperature on obtainable conversion efficiency in n-ZnO/p-Cu2O solar cells." Thin Solid Films 528(0): 72-76.

Norlin, A., J. Pan and C. Leygraf (2002). "Investigation of interfacial capacitance of Pt, Ti and TiN coated electrodes by electrochemical impedance spectroscopy." Biomolecular Engineering 19(2–6): 67-71.

Novoselov, K. S., A. K. Geim, S. V. Morozov, D. Jiang, Y. Zhang, S. V. Dubonos, I. V. Grigorieva and A. A. Firsov (2004). "Electric Field Effect in Atomically Thin Carbon Films." Science 306(5696): 666-669.

Nowotny, M. K., P. Bogdanoff, T. Dittrich, S. Fiechter, A. Fujishima and H. Tributsch (2010). "Observations of p-type semiconductivity in titanium dioxide at room temperature." Materials Letters 64(8): 928-930.

O'Regan, B. and M. Graetzel (1991). "Low-cost, high-efficiency solar cell based on dye-sensitized colloidal TiO2 films." Nature 353(6346): 737.

O'Regan, B. and M. Gratzel (1991). "A low-cost, high-efficiency solar cell based on dye-sensitized colloidal TiO2 films." Nature 353(6346): 737-740.

Pan, N., D. Guan, Y. Yang, Z. Huang, R. Wang, Y. Jin and C. Xia (2014). "A rapid low-temperature synthetic method leading to large-scale carboxyl graphene." Chemical Engineering Journal 236(0): 471-479.

Parisi, M. L., S. Maranghi and R. Basosi (2014). "The evolution of the dye sensitized solar cells from Grätzel prototype to up-scaled solar applications: A life cycle assessment approach." Renewable and Sustainable Energy Reviews 39(0): 124-138.

Park, H. S., M. H. Lee, R. Y. Hwang, O. K. Park, K. Jo, T. Lee, B. S. Kim and H. K. Song (2014). "Kinetically enhanced pseudocapacitance of conducting polymer doped with reduced graphene oxide through a miscible electron transfer interface." Nano Energy 3(0): 1-9.

Park, S. and R. S. Ruoff (2009). "Chemical methods for the production of graphenes." Nat Nano 4(4): 217-224.

Parthiban, R., D. Balamurugan and B. G. Jeyaprakash (2015). "Spray deposited ZnO and Ga doped ZnO based DSSC with bromophenol blue dye as sensitizer: Efficiency analysis through DFT approach." Materials Science in Semiconductor Processing 31(0): 471-477.

Pavithra, N., A. M. Asiri and S. Anandan (2015). "Fabrication of dye sensitized solar cell using gel polymer electrolytes consisting

poly(ethylene oxide)-acetamide composite." Journal of Power Sources 286(0): 346-353.

Peng, S., L. Li, H. Tan, M. Srinivasan, S. G. Mhaisalkar, S. Ramakrishna and Q. Yan (2013). "Platinum/polyaniline transparent counter electrodes for quasi-solid dye-sensitized solar cells with electrospun PVDF-HFP/TiO2 membrane electrolyte." Electrochimica Acta 105(0): 447-454.

Peng, S., Y. Wu, P. Zhu, V. Thavasi, S. G. Mhaisalkar and S. Ramakrishna (2011). "Facile fabrication of polypyrrole/functionalized multiwalled carbon nanotubes composite as counter electrodes in low-cost dye-sensitized solar cells." Journal of Photochemistry and Photobiology A: Chemistry 223(2–3): 97-102.

Peng, Y. J., T.-H. Wu, C. T. Hsu, S. M. Li, M. G. Chen and C. C. Hu (2014). "Electrochemical characteristics of the reduced graphene oxide/carbon nanotube/polypyrrole composites for aqueous asymmetric supercapacitors." Journal of Power Sources 272(0): 970-978.

Qi, K., Y. Qiu and X. Guo (2014). "Pulse electrochemical incorporation of graphene oxide into polypyrrole films for supercapacitor electrode materials." Electrochimica Acta 137(0): 685-692.

Qin, H., Y. Xu, J. Kim, T. Hwang and T. Kim (2014). "The effect of structure on the photoactivity of a graphene/TiO2 composite." Materials Science and Engineering: B 184(0): 72-79.

Qiu, L., H. Zhang, W. Wang, Y. Chen and R. Wang "Effects of hydrazine hydrate treatment on the performance of reduced graphene oxide film as counter electrode in dye-sensitized solar cells." Applied Surface Science(0).

Rajesh, W. Takashima and K. Kaneto (2004). "Amperometric tyrosinase based biosensor using an electropolymerized PTS-doped polypyrrole film as an entrapment support." Reactive and Functional Polymers 59(2): 163-169.

Raksa, P., S. Nilphai, A. Gardchareon and S. Choopun (2009). "Copper oxide thin film and nanowire as a barrier in ZnO dye-sensitized solar cells." Thin Solid Films 517(17): 4741-4744.

Ranjitha, A., N. Muthukumarasamy, M. Thambidurai, R. Balasundaraprabhu and S. Agilan (2013). "Effect of annealing temperature on nanocrystalline TiO2 thin films prepared by sol–gel dip coating method." Optik - International Journal for Light and Electron Optics 124(23): 6201-6204.

Rao, C. N. R., K. Biswas, K. S. Subrahmanyam and A. Govindaraj (2009). "Graphene, the new nanocarbon." Journal of Materials Chemistry 19: 2457-2469.

Raudsepp, T., M. Marandi, T. Tamm, V. Sammelselg and J. Tamm (2010). "Redoping - A simple way to enhance the redoxcapacity of polypyrrole films." Electrochemistry Communications 12(9): 1180-1183.

Ren, C., B. Yang, M. Wu, J. Xu, Z. Fu, Y. lv, T. Guo, Y. Zhao and C. Zhu (2010). "Synthesis of Ag/ZnO nanorods array with enhanced photocatalytic performance." Journal of Hazardous Materials 182(1-3): 123-129.

Saha, B., N. S. Das and K. K. Chattopadhyay (2014). "Combined effect of oxygen deficient point defects and Ni doping in radio frequency magnetron sputtering deposited ZnO thin films." Thin Solid Films 562(0): 37-42.

Sahay, R., J. Sundaramurthy, P. Suresh Kumar, V. Thavasi, S. G. Mhaisalkar and S. Ramakrishna (2012). "Synthesis and characterization of CuO nanofibers, and investigation for its suitability as blocking layer in ZnO NPs based dye sensitized solar cell and as photocatalyst in organic dye degradation." Journal of Solid State Chemistry 186(0): 261-267.

Sahu, D. R., S. Y. Lin and J. L. Huang (2006). "ZnO/Ag/ZnO multilayer films for the application of a very low resistance transparent electrode." Applied Surface Science 252(20): 7509-7514.

Salhi, R., R. Maalej, M. Fourati, Y. Guyot, O. Chaix-Pluchery, L. Rapenne, C. Jimenez and J. L. Deschanvres (2011). "Influence of deposition conditions on the optical properties of erbium-doped yttrium oxide films grown by aerosol–UV assisted MOCVD." Journal of Luminescence 131(11): 2311-2316.

Saranya, K., M. Rameez and A. Subramania "Developments in conducting polymer based counter electrodes for dye-sensitized solar cells - An overview." European Polymer Journal(0).

Saranya, K., M. Rameez and A. Subramania (2015). "Developments in conducting polymer based counter electrodes for dye-sensitized solar cells – An overview." European Polymer Journal 66(0): 207-227.

Saravanan, R., M. Mansoob Khan, V. K. Gupta, E. Mosquera, F. Gracia, V. Narayanan and A. Stephen (2015). "ZnO/Ag/CdO nanocomposite for visible light-induced photocatalytic degradation of industrial textile effluents." Journal of Colloid and Interface Science 452(0): 126-133.

Shaikh, S. F., R. S. Mane, Y. J. Hwang and O. S. Joo (2015). "Calcium carbonate electronic-insulating layers improve the charge collection

efficiency of tin oxide photoelectrodes in dye-sensitized solar cells." Electrochimica Acta 167(0): 379-387.

Shan, C. H., X. J. Sang, H. Zhang, J. S. Li, W. L. Chen, Z. M. Su and E. B. Wang (2014). "Enhanced DSSC performance with tri-pyridine-ruthenium heteropolytungstate." Inorganic Chemistry Communications 50(0): 13-16.

Sharma, G. D., D. Daphnomili, P. A. Angaridis, S. Biswas and A. G. Coutsolelos (2013). "Effect of thiourea incorporation in the electrolyte on the photovoltaic performance of the DSSC sensitized with pyridyl functionalized porphyrin." Electrochimica Acta 102(0): 459-465.

Sharma, G. D., M. L. Keshtov, A. R. Khokhlov, D. Tasis and C. Galiotis (2014). "Improved power conversion efficiency by insertion of RGO–TiO2 composite layer as optical spacer in polymer bulk heterojunction solar cells." Organic Electronics 15(2): 348-355.

Shi, M., X. Pan, W. Qiu, D. Zheng, M. Xu and H. Chen (2011). "Si/ZnO core–shell nanowire arrays for photoelectrochemical water splitting." International Journal of Hydrogen Energy 36(23): 15153-15159.

Sultana, I., M. M. Rahman, S. Li, J. Wang, C. Wang, G. G. Wallace and H.-K. Liu (2012). "Electrodeposited polypyrrole (PPy)/para (toluene sulfonic acid) (pTS) free-standing film for lithium secondary battery application." Electrochimica Acta 60(0): 201-205.

Sultana, I., M. M. Rahman, J. Wang, C. Wang, G. G. Wallace and H. K. Liu (2012). "All-polymer battery system based on polypyrrole (PPy)/para (toluene sulfonic acid) (pTS) and polypyrrole (PPy)/indigo carmine (IC) free standing films." Electrochimica Acta 83(0): 209-215.

Sun, B., L. Chen, Y. Xu, M. Liu, H. Yin and S. Ai (2014). "Ultrasensitive photoelectrochemical immunoassay of indole-3-acetic acid based on the MPA modified CdS/RGO nanocomposites decorated ITO electrode." Biosensors and Bioelectronics 51(0): 164-169.

Sun, W. and Z. Mo (2013). "PPy/graphene nanosheets/rare earth ions: A new composite electrode material for supercapacitor." Materials Science and Engineering: B 178(8): 527-532.

Sun, W., X. Sun, T. Peng, Y. Liu, H. Zhu, S. Guo and X. Z. Zhao (2012). "A low cost mesoporous carbon/SnO2/TiO2 nanocomposite counter electrode for dye-sensitized solar cells." Journal of Power Sources 201(0): 402-407.

Sun, X., Q. Zhang, Y. Liu, N. Huang, P. Sun, T. Peng, T. Peng and X.-Z. Zhao (2014). "Photovoltaic performance improvement of dye-sensitized solar cells through introducing In-doped TiO2 film at conducting glass and mesoporous TiO2 interface as an efficient compact layer." Electrochimica Acta 129(0): 276-282.

Tamburri, E., V. Guglielmotti, S. Orlanducci and M. L. Terranova (2011). "Structure and I2/I− redox catalytic behaviour of PEDOT–PSS films electropolymerized in aqueous medium: Implications for convenient counter electrodes in DSSC." Inorganica Chimica Acta 377(1): 170-176.

Tripathi, S. K., M. Rani and N. Singh (2015). "ZnO:Ag and TZO:Ag Plasmonic Nanocomposite for Enhanced Dye Sensitized Solar Cell Performance." Electrochimica Acta 167(0): 179-186.

Ul Haq, E., S. Kunjalukkal Padmanabhan and A. Licciulli (2015). "Microwave synthesis of thermal insulating foams from coal derived bottom ash." Fuel Processing Technology 130(0): 263-267.

Ullah, K., Z. D. Meng, S. Ye, L. Zhu and W. C. Oh (2014). "Synthesis and characterization of novel PbS–graphene/TiO2 composite with enhanced photocatalytic activity." Journal of Industrial and Engineering Chemistry 20(3): 1035-1042.

Veerender, P., V. Saxena, P. Jha, S. P. Koiry, A. Gusain, S. Samanta, A. K. Chauhan, D. K. Aswal and S. K. Gupta (2012). "Free-standing polypyrrole films as substrate-free and Pt-free counter electrodes for quasi-solid dye-sensitized solar cells." Organic Electronics 13(12): 3032-3039.

Vera, R., R. Schrebler, P. Grez and H. Romero (2014). "The corrosion-inhibiting effect of polypyrrole films doped with p-toluene-sulfonate, benzene-sulfonate or dodecyl-sulfate anions, as coating on stainless steel in NaCl aqueous solutions." Progress in Organic Coatings 77(4): 853-858.

Wang, D., X. Li, J. Chen and X. Tao (2012). "Enhanced photoelectrocatalytic activity of reduced graphene oxide/TiO2 composite films for dye degradation." Chemical Engineering Journal 198–199(0): 547-554.

Wang, G., Y. Ling, H. Wang, L. Xihong and Y. Li (2014). "Chemically modified nanostructures for photoelectrochemical water splitting." Journal of Photochemistry and Photobiology C: Photochemistry Reviews 19(0): 35-51.

Wang, G., B. Wang, J. Park, Y. Wang, B. Sun and J. Yao (2009). "Highly efficient and large-scale synthesis of graphene by electrolytic exfoliation." Carbon 47(14): 3242-3246.

Wang, H. F., L. Y. Chen, W. N. Su, J. C. Chung and B. J. Hwang (2010). "Effect of the Compact TiO2 Layer on Charge Transfer between N3 Dyes and TiO2 Investigated by Raman Spectroscopy." The Journal of Physical Chemistry C 114(7): 3185-3189.

Wang, P., J. Wang, X. Wang, H. Yu, J. Yu, M. Lei and Y. Wang (2013). "One-step synthesis of easy-recycling TiO2-rGO nanocomposite photocatalysts with enhanced photocatalytic activity." Applied Catalysis B: Environmental 132–133(0): 452-459.

Wang, Q., S. Ito, M. Grätzel, F. Fabregat-Santiago, I. Mora-Seró, J. Bisquert, T. Bessho and H. Imai (2006). "Characteristics of High Efficiency Dye-Sensitized Solar Cells†." The Journal of Physical Chemistry B 110(50): 25210-25221.

Wang, R., J. Sun, L. Gao, C. Xu, J. Zhang and Y. Liu (2011). "Effective post treatment for preparing highly conductive carbon nanotube/reduced graphite oxide hybrid films." Nanoscale 3(3): 904-906.

Wang, X., Y. Fang, L. He, Q. Wang and T. Wu (2014). "Influence of compact TiO2 layer on the photovoltaic characteristics of the organometal halide perovskite-based solar cells." Materials Science in Semiconductor Processing 27(0): 569-576.

Wang, Y. F., W. X. Zhao, X. F. Li and D. J. Li (2015). "Engineered Interfacial and Configuration Design of Double Layered SnO2@TiO2-ZnO Nanoplates Ternary Heterostructures for Efficient Dye-Sensitized Solar Cells." Electrochimica Acta 151(0): 399-406.

Wu, J., Q. Li, L. Fan, Z. Lan, P. Li, J. Lin and S. Hao (2008). "High-performance polypyrrole nanoparticles counter electrode for dye-sensitized solar cells." Journal of Power Sources 181(1): 172-176.

Wu, Z., H. Wang, Y. Liu and Z. Gu (2008). "Photocatalytic oxidation of nitric oxide with immobilized titanium dioxide films synthesized by hydrothermal method." Journal of Hazardous Materials 151(1): 17-25.

Xian, F., K. Miao, X. Bai, Y. Ji, F. Chen and X. Li (2013). "Characteraction of Ag-doped ZnO thin film synthesized by sol–gel method and its using in thin film solar cells." Optik - International Journal for Light and Electron Optics 124(21): 4876-4879.

Xu, G., H. Liu, J. Wang, J. Lv, Z. Zheng and Y. Wu (2014). "Photoelectrochemical Performances and Potential Applications of TiO2 Nanotube Arrays Modified with Ag and Pt Nanoparticles." Electrochimica Acta 121(0): 194-202.

Xu, J. L., L. Z. Bao, A. H. Liu, X. J. Jin, Y. X. Tong, J. M. Luo, Z. C. Zhong and Y. F. Zheng (2015). "Microstructure, mechanical properties and superelasticity of biomedical porous NiTi alloy prepared by microwave sintering." Materials Science and Engineering: C 46(0): 387-393.

Yang, C. C., H. Q. Zhang and Y. R. Zheng (2011). "DSSC with a novel Pt counter electrodes using pulsed electroplating techniques." Current Applied Physics 11(1, Supplement): S147-S153.

Yang, H., P. Li, J. Zhang and Y. Lin (2014). "TiO2 compact layer for dye-sensitized SnO2 nanocrystalline thin film." Electrochimica Acta 147(0): 366-370.

Yang, J., X. Shen, Z. Ji, H. Zhou, G. Zhu and K. Chen (2015). "In-situ growth of Cu nanoparticles on reduced graphene oxide nanosheets and their excellent catalytic performance." Ceramics International 41(3, Part A): 4056-4063.

Yang, Y., X. Peng, S. Chen, L. Lin, B. Zhang and Y. Feng (2014). "Performance improvement of dye-sensitized solar cells by introducing a hierarchical compact layer involving ZnO and TiO2 blocking films." Ceramics International 40(9, Part B): 15199-15206.

Yong, S. M., N. Tsvetkov, L. Larina, B. T. Ahn and D. K. Kim (2014). "Ultrathin SnO2 layer for efficient carrier collection in dye-sensitized solar cells." Thin Solid Films 556(0): 503-508.

Yoon, C. O., H. K. Sung, J. H. Kim, E. Barsoukov, J. H. Kim and H. Lee (1999). "The effect of low-temperature conditions on the electrochemical polymerization of polypyrrole films with high density, high electrical conductivity and high stability." Synthetic Metals 99(3): 201-212.

Yue, G., L. Wang, X. a. Zhang, J. Wu, Q. Jiang, W. Zhang, M. Huang and J. Lin (2014). "Fabrication of high performance multi-walled carbon nanotubes/polypyrrole counter electrode for dye-sensitized solar cells." Energy 67(0): 460-467.

Yue, G., X. a. Zhang, L. Wang, F. Tan, J. Wu, Q. Jiang, J. Lin, M. Huang and Z. Lan (2014). "Highly efficient and stable dye-sensitized solar cells based on nanographite/polypyrrole counter electrode." Electrochimica Acta 129(0): 229-236.

Zeng, X., J. Bao, M. Han, W. Tu and Z. Dai (2014). "Quantum dots sensitized titanium dioxide decorated reduced graphene oxide for visible light excited photoelectrochemical biosensing at a low potential." Biosensors and Bioelectronics 54(0): 331-338.

Zhang, F., J. Zhao, T. Shen, H. Hidaka, E. Pelizzetti and N. Serpone (1998). "TiO2-assisted photodegradation of dye pollutants II. Adsorption and degradation kinetics of eosin in TiO2 dispersions under visible light irradiation." Applied Catalysis B: Environmental 15(1–2): 147-156.

Zhang, L., N. Li, H. Jiu, G. Qi and Y. Huang (2015). "ZnO-reduced graphene oxide nanocomposites as efficient photocatalysts for

photocatalytic reduction of CO2." Ceramics International 41(5, Part A): 6256-6262.

Zhang, Q., K. Zhang, D. Xu, G. Yang, H. Huang, F. Nie, C. Liu and S. Yang (2014). "CuO nanostructures: Synthesis, characterization, growth mechanisms, fundamental properties, and applications." Progress in Materials Science 60(0): 208-337.

Zhang, Z., M. F. Hossain, T. Arakawa and T. Takahashi (2010). "Facing-target sputtering deposition of ZnO films with Pt ultra-thin layers for gas-phase photocatalytic application." Journal of Hazardous Materials 176(1–3): 973-978.

Zhao, W., H. Bala, J. Chen, Y. Zhao, G. Sun, J. Cao and Z. Zhang (2013). "Thickness-dependent electron transport performance of mesoporous TiO2 thin film for dye-sensitized solar cells." Electrochimica Acta 114(0): 318-324.

Zheng, J. Y., G. Song, C. W. Kim and Y. S. Kang (2012). "Facile preparation of p-CuO and p-CuO/n-CuWO4 junction thin films and their photoelectrochemical properties." Electrochimica Acta 69(0): 340-344.

Zhong, P., W. Que, Y. Liao, J. Zhang and X. Hu (2012). "Improved performance in dye-sensitized solar cells by rationally tailoring anodic TiO2 nanotube length." Journal of Alloys and Compounds 540(0): 159-164.

Zhou, Y., C. Xia, X. Hu, W. Huang, A. A. Aref, B. Wang, Z. Liu, Y. Sun, W. Zhou and Y. Tang (2014). "Dye-sensitized solar cells based on nanoparticle-decorated ZnO/SnO2 core/shell nanoneedle arrays." Applied Surface Science 292(0): 111-116.

Zhu, M., X. Li, W. Liu and Y. Cui (2014). "An investigation on the photoelectrochemical properties of dye-sensitized solar cells based on graphene–TiO2 composite photoanodes." Journal of Power Sources 262(0): 349-355.

Zhu, S., X. Tian, L. Shan, Z. Ding, Z. Kan, X. Xu, Z. Zhou and L. Wang (2013). "Effect of Al3+ on the growth of ZnO nanograss film and its application in dye-sensitized solar cells." Ceramics International 39(8): 9637-9644.

Zhu, Y., X. Xu, L. Zhang, J. Chen and Y. Cao (2012). "High efficiency inverted polymeric bulk-heterojunction solar cells with hydrophilic conjugated polymers as cathode interlayer on ITO." Solar Energy Materials and Solar Cells 97(0): 83-88.

BIODATA OF STUDENT

The MSc student, Nor Fathin Aini Jumeri was born in Selangor, Malaysia on 10th June 1989. She received her primary education level at SK Taman Muda, Ampang and SK (2) Taman Keramat, Kuala Lumpur. She received her secondary education at SMK Assunta, Petaling Jaya and SMK Desa Tun Hussein Onn, Kuala Lumpur. Her pre-university education was at Kolej Matrikulasi Johor. Later, she received an admission offer for Bachelor Degree in Chemistry in 2009 at Universiti Putra Malaysia, Serdang Campus and after 4 years, was successfully awarded with the Bachelor of Science (Honours) in Chemistry with a second class upper honour. She pursued a Degree of Master in Material Science at the same university. Her contact details are as follow:

Address: No 23, Jalan AU2A, Taman Seri Keramat, 54200, Kuala Lumpur, Malaysia.

Contact number: 017-6983490

Email: fathinainijumeri@gmail.com

LIST OF PUBLICATIONS

1. Article Title : Titanium Dioxide-Reduced Graphene Oxide Thin Film for Photoelectrochemical Water Splitting
   Journal : Ceramics International
   Publisher : Elsevier
   Volume : Volume 40, Article ID 176825

2. Article Title : Dual Functional Reduced Graphene Oxide as Photoanode and Counter Electrode in Dye-Sensitized Solar Cells and Its Exceptional Efficiency Enhancement
   Journal : Journal of Power Sources
   Publisher : Elsevier
   Volume : Volume 293, Article ID 01791

CONFERENCE ATTENDED

1. Name of Conference: The Regional Fundamental Science Congress 2014, 19-20 August 2014,UPM, Selangor.
   Project Title : Titanium Dioxide-Reduced Graphene Oxide Thin Film for Photoelectrochemical Water Splitting (Oral Presenter).

2. Name of Conference : Regional Conference on Solid State Science and Technology 2014, 25-27 November 2014, Cameron Highland, Pahang.
   Project Title : Titanium Dioxide-Reduced Graphene Oxide Thin Film for Photoelectrochemical Water Splitting.

UNIVERSITI PUTRA MALAYSIA

STATUS CONFIRMATION FOR THESIS / PROJECT REPORT AND COPYRIGHT

ACADEMIC SESSION : _____

TITLE OF THESIS / PROJECT REPORT :

_____

_____

_____

NAME OF STUDENT :

_____

I acknowledge that the copyright and other intellectual property in the thesis/project report belonged to Universiti Putra Malaysia and I agree to allow this thesis/project report to be placed at the library under the following terms:

1. This thesis/project report is the property of Universiti Putra Malaysia.
2. The library of Universiti Putra Malaysia has the right to make copies for educational purposes only.
3. The library of Universiti Putra Malaysia is allowed to make copies of this thesis for academic exchange.

I declare that this thesis is classified as:

*Please tick (√)

☐	**CONFIDENTIAL**	(Contain confidential information under Official Secret Act 1972).
☐	**RESTRICTED**	(Contains restricted information as specified by the organization/institution where research was done).
☐	**OPEN ACCESS**	I agree that my thesis/project report to be published as hard copy or online open access.

This thesis is submitted for:

☐ **PATENT** Embargo from _____ until _____
(date) (date)

Approved by:

_____ _____
(Signature of Student) (Signature of Chairman
New IC No/ Passport No.: of Supervisory Committee)
Name:

Date : Date :

[Note : If the thesis is CONFIDENTIAL or RESTRICTED, please attach with the letter from the organization/institution with period and reasons for confidentially or restricted.]